

A Survey on Deep Learning-Based Monocular Spacecraft Pose Estimation: Current State, Limitations and Prospects

Leo Pauly Wassim Rharbaoui Carl Shneider
Arunkumar Rathinam Vincent Gaudillière Djamila Aouada

Abstract—Estimating the pose of an uncooperative spacecraft is an important computer vision problem for enabling the deployment of automatic vision-based systems in orbit, with applications ranging from on-orbit servicing to space debris removal. Following the general trend in computer vision, more and more works have been focusing on leveraging Deep Learning (DL) methods to address this problem. However and despite promising research-stage results, major challenges preventing the use of such methods in real-life missions still stand in the way. In particular, the deployment of such computation-intensive algorithms is still under-investigated, while the performance drop when training on synthetic and testing on real images remains to mitigate. The primary goal of this survey is to describe the current DL-based methods for spacecraft pose estimation in a comprehensive manner. The secondary goal is to help define the limitations towards the effective deployment of DL-based spacecraft pose estimation solutions for reliable autonomous vision-based applications. To this end, the survey first summarises the existing algorithms according to two approaches: hybrid modular pipelines and direct end-to-end regression methods. A comparison of algorithms is presented not only in terms of pose accuracy but also with a focus on network architectures and models’ sizes keeping potential deployment in mind. Then, current monocular spacecraft pose estimation datasets used to train and test these methods are discussed. The data generation methods: simulators and testbeds, the domain gap and the performance drop between synthetically generated and lab/space collected images and the potential solutions are also discussed. Finally, the paper presents open research questions and future directions in the field, drawing parallels with other computer vision applications.

Index Terms—Spacecraft Pose Estimation, Algorithms, Deep Learning, Datasets, Simulators and Testbeds, Domain adaptation.

I. INTRODUCTION

In recent years, the number of satellites launched into orbit has increased rapidly, aided by lower launch costs and minimal entry barriers, making space more accessible than ever before [1], [2]. Each space mission has a unique set of goals that influences the satellite’s size, functions, and intended lifetime. In most mission scenarios, the satellites launched into orbit will last for the entire mission life-cycle, and at the end of life, they are either moved to the

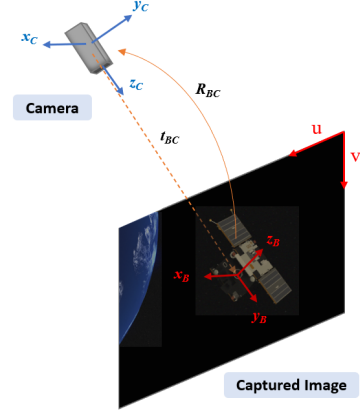


Fig. 1: Spacecraft pose estimation is the problem of finding the relative position (t_{BC}) and orientation (R_{BC}) of the target spacecraft reference frame (B) shown in red, with respect to the camera reference frame (C) shown in blue, mounted on a chaser spacecraft.

graveyard orbit or left to re-enter the Earth’s atmosphere. However, a few space missions may encounter anomalies or malfunctions before their full life span. These malfunctioned satellites may become non-cooperative and threaten existing space infrastructure. To tackle such scenarios, the demand for orbital missions targeting On-Orbit Servicing (OOS) and Active Debris Removal (ADR) has steadily increased, as OOS and ADR are considered key spaceflight capabilities for the next decade. OOS is defined as the process of inspection, maintenance, and repair of a system as an in-space operation. Commercial OOS missions aim to perform various functions, including providing life extension, maintaining the spacecraft, rescuing and recovering satellites from deployment failures and assisting astronauts with extravehicular activities [3], [4]. ADR is the process of removing obsolete space objects (such as satellites, rocket bodies, or fragments of spacecraft) through an external disposal method, thus minimizing the build-up of unnecessary objects and lowering the probability of on-orbit collisions that can fuel a “collision cascade” [5], [6]. Several technology demonstration missions, including PROBA-3 by the European Space Agency (ESA) [7], PRISMA by OHB Sweden [8], and commercial missions such as MEV-1 by

All authors are affiliated to the Computer Vision, Imaging & Machine Intelligence Research Group (CVI²) at the Interdisciplinary Centre for Security, Reliability and Trust (SnT), University of Luxembourg, Luxembourg.

Northrop Grumman [9], had been carried out successfully in recent years. Future missions such as Clearspace-1 by ESA and Clearspace [10] are already in preparation to demonstrate ADR in 2026.

An important aspect of OOS and ADR missions is that it requires rendezvous and proximity operations near the target before performing mission-specific operations. To perform any rendezvous operations, it is essential to know the target spacecraft's position and orientation (i.e. pose), allowing the relative navigation algorithms to generate real-time trajectories onboard the spacecraft. Several sensor options are available to perform inference and observation of the target spacecraft state, including Monocular RGB/Greyscale Cameras, Stereo Cameras, Thermal cameras, Range Detection and Ranging (RADAR), Light Detection and Ranging (LIDAR), etc. Monocular cameras are widely preferred over other active sensors (like LIDARs and RADARs) due to their relative simplicity, small size, weight, power requirements, and ability to be easily integrated into a wide range of spacecraft configurations.

Recovering the relative pose between a camera and an observed object from a single image is a fundamental computer vision problem [11]–[13]. Given an image and the corresponding intrinsic camera parameters, the relative pose estimation problem involves estimating the relative transformation, i.e. translation and rotation, between the camera and the target object. The location of the object in the camera reference frame is specified by $t \in \mathbb{R}^3$, and its orientation is most often represented by a quaternion $q = (q_0, q_1, q_2, q_3) \in \mathbb{R}^4$. The relative orientation (rotation) can also be represented using standard 3D rotation representations such as rotation matrix or Euler's Angles [14]. In Figure 1, a simple illustration of the spacecraft pose estimation problem is presented, where axes x_C, y_C, z_C represent the camera reference frame mounted on the chaser (C) spacecraft and x_B, y_B, z_B represent the target spacecraft's body (B) reference frame. Spacecraft pose estimation is the problem of finding the relative position (t_{BC}) and orientation (R_{BC}) of the reference frame of a target spacecraft with respect to the reference frame of a camera mounted on a chaser spacecraft, using a single image from a monocular camera.

In the last decade, vision-based spacecraft pose estimation has utilized hand-engineered features described using feature descriptors and detected using feature detectors to detect these features in the 2D images and to finally use their 3D correspondences to find the relative pose [15], [16]. Although the use of feature correspondences between the detected features in the 2D image and 3D feature locations, together with perspective transformation, aids in pose solution convergence, the features are not robust to harsh lighting conditions encountered in space. The feature-based approaches perform poorly in variable illumination conditions, low signal-to-noise ratio, and high contrast characteristics encountered in space imagery. This results in a poor estimation of the target state in many scenarios. Spacecraft pose estimation before the evolution of deep learning algorithms has been summarised in [17],

[18]. With their gain in popularity and exponential growth, Deep Learning (DL)-based approaches have prompted many new developments in recent years. According to the findings of the recent ESA's Spacecraft Pose Estimation Challenges [19], [20], DL-based methods have been the preferred option for tackling the problem of uncooperative spacecraft pose estimation. However, investigated DL-based approaches still heavily rely on annotated data that are cumbersome to obtain. While synthetic data generation and laboratory data acquisition have been identified as the most tractable way to train and test such algorithms, the performance drops significantly on the test image domain compared to the train image domain, such problem being known as the *domain gap* [21]. Dedicated strategies have therefore to be investigated to mitigate it. In addition, the laboratory conditions under which test images are acquired still differ from space-borne conditions, adding another level of domain discrepancy that is yet to be addressed.

A recent survey on the DL-based approaches for spacecraft relative navigation [22] provides a general narrative across different use cases, including spacecraft pose estimation. In this survey, we focus on monocular pose estimation of non-cooperative targets using DL approaches and review the latest developments in the field. In addition, we conduct a comparison between the two main types of approaches and assess the still unmet needs that would enable the deployment of DL-based algorithms in real space missions. Furthermore, we explore the fundamental counterpart of any DL-based algorithm that is the data. We review the existing datasets, generation engines and testbed facilities. We also analyse the current validation procedure that consists in testing on laboratory-acquired images algorithms trained on synthetic data, after discussing the methods proposed to address this domain gap. Finally, we provide the reader with prospects on research directions that could help making the leap to the deployment of reliable DL-based spacecraft pose estimation algorithms for autonomous in-orbit operations.

The following sections are organized as follows. Section II provides a comprehensive survey of the two main types of DL-based algorithms for spacecraft pose estimation, before highlighting their limitations. Section III presents the datasets, generation engines and testbed facilities. It also presents the main existing methods to address the domain gap between synthetic and laboratory images, and discuss the underlying validation procedure. Section IV discusses open research problems and future directions and finally, Section V concludes the survey.

II. ALGORITHMS

The use of DL has had significant implications in developing computer vision algorithms over the last decade [46], [47], improving their performance and robustness for applications such as image classification [48], segmentation [49], and object tracking [50]. Following this trend, the proposals of DL-based spacecraft pose estimation algorithms have outnumbered [22], [17] the classical feature-engineering-based methods [51]–[56] in recent years. Figure 2 presents an overview

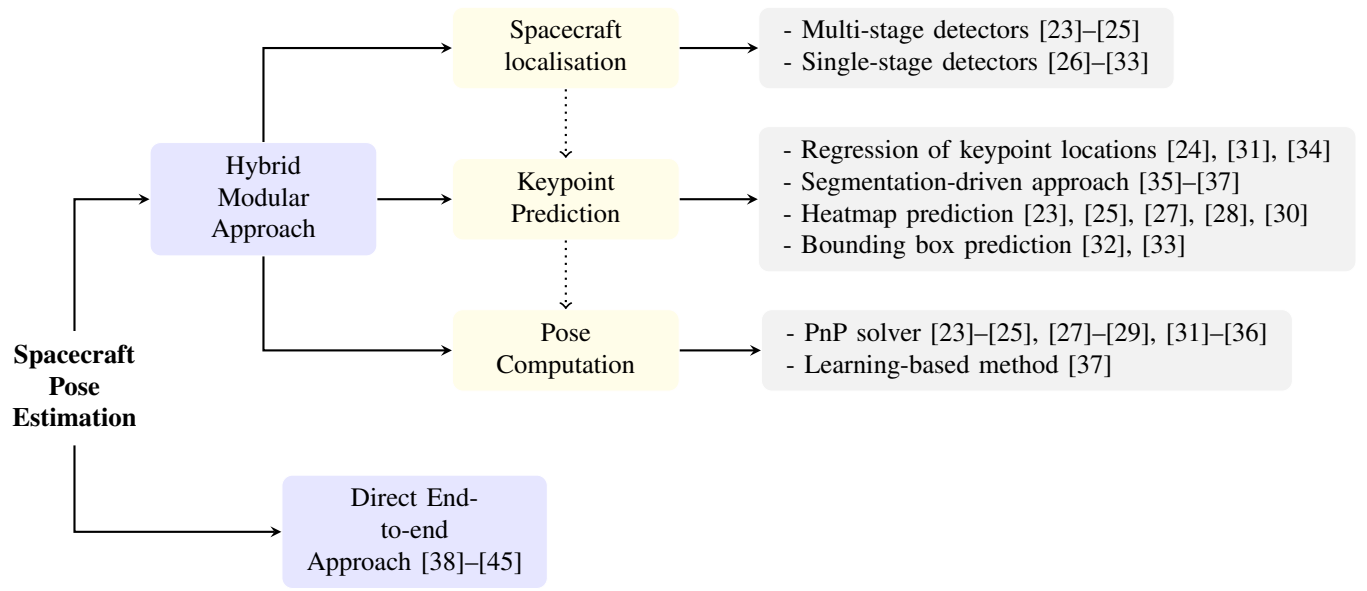


Fig. 2: Tree diagram of spacecraft pose estimation algorithms reviewed in this paper. Blue boxes show the two different categories of approaches: hybrid modular and direct end-to-end. The yellow boxes and the sub-branches (grey boxes) show the separate stages and the different methods used at each stage, respectively, of the hybrid modular approach.

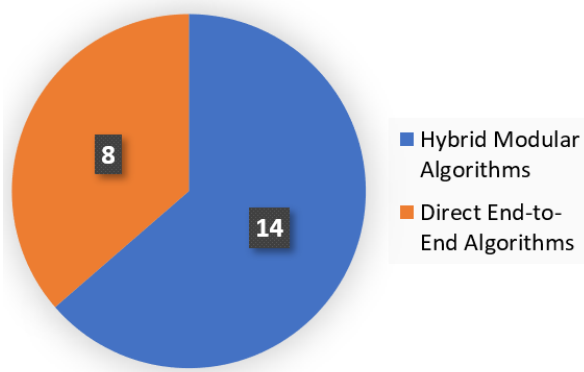


Fig. 3: Distribution of algorithms surveyed in this paper

tree diagram of the algorithms reviewed in this survey and Figure 3 shows their branching into different approaches. DL-based spacecraft pose estimation algorithms broadly fall under two categories: 1) Hybrid modular approaches, and 2) Direct end-to-end approaches.

Hybrid modular approaches (see Figure 4-A) combine multiple DL models and classical computer vision methods for spacecraft pose estimation. On the other hand, direct end-to-end approaches (see Figure 4-B) only use a single DL model for pose estimation, trained end-to-end. Each of these approaches are discussed in detail (Section II-A and Section II-B), with a comparative analysis (Section II-C) and a discussion on limitations (Section II-D) below.

A. Hybrid Modular Approaches

This survey defines hybrid approaches as those using a combination of DL models and classical computer vision

methods for spacecraft pose estimation. The hybrid algorithms have three common stages (see Figure 5): (1) *spacecraft localisation* for detecting and cropping the spacecraft region in the image, (2) *keypoint prediction* for predicting 2D keypoints locations of pre-defined 3D keypoints inside cropped regions and (3) *pose computation* for computing the pose from these 2D-3D correspondences. The following subsections describe each of these stages in detail.

1) *Spacecraft Localisation*: The spacecraft object size in the image varies considerably with changes in the relative distance between the chaser and target spacecraft as illustrated in Figure 6. This scale variance affects the performance of the pose estimation algorithm [19]. The spacecraft localisation stage uses a DL object detection framework to detect the spacecraft by predicting bounding boxes around the object (spacecraft). These bounding boxes are then used to crop out the region of interest (RoI) in the image containing the spacecraft. The extracted RoI is then processed for pose estimation in the subsequent stages. Based on literature [58], DL-based object detectors for spacecraft localisation can be classified into two categories:

- Multi-stage object detectors
- Single-stage object detectors

Multi-stage object detectors: In these detectors object detection proceeds in multiple stages. The first stage generates region proposals, i.e. image areas with a higher probability of containing objects to be detected. These region proposals are then refined and classified in the second stage. Detectors of this kind generally provide highly accurate detections. However, due to their multi-stage nature, they suffer from longer image processing times (high latency) and higher number of parameters making them resource-intensive. This can

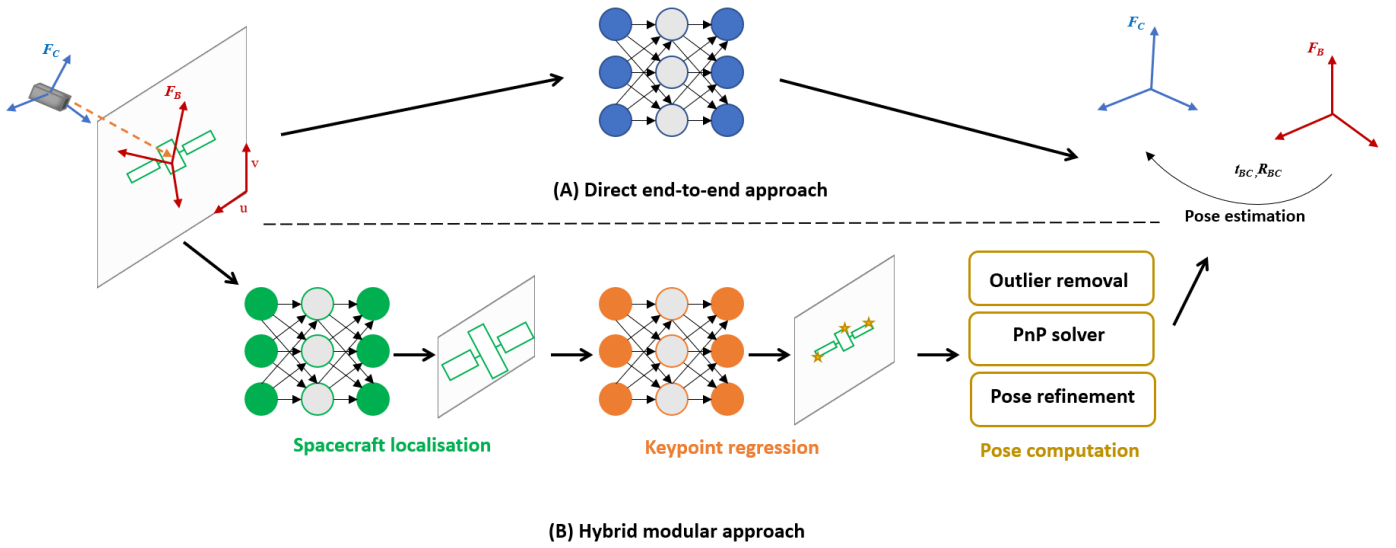


Fig. 4: Illustration of different approaches for spacecraft pose estimation. A) Direct end-to-end approaches which use deep learning. B) Hybrid modular approaches which consist of three steps: object detection/localisation, keypoint regression, and pose computation. The first two steps use deep learning and the third step uses a classical algorithm which performs outlier removal necessary for the PnP solver and finally pose refinement.

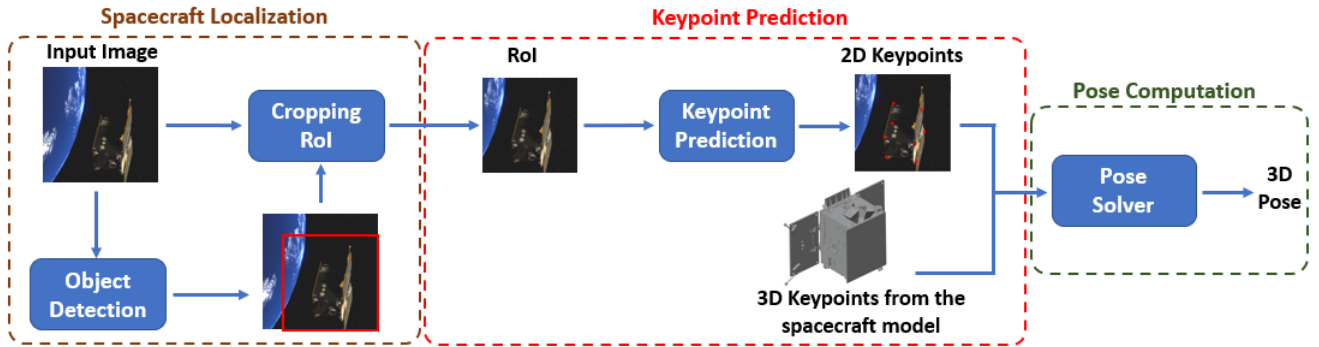


Fig. 5: Hybrid modular approach for spacecraft pose estimation. The spacecraft localisation stage is outlined in blue, the keypoint prediction stage is in red and the pose computation stage is shown in green. Spacecraft image from the SPARK2 dataset is used for illustration [57].

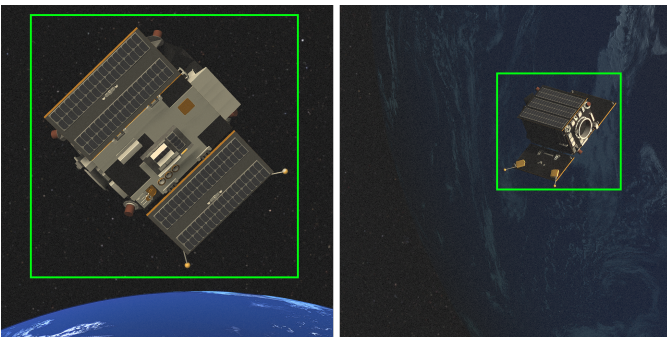


Fig. 6: Illustrating variations in spacecraft size in captured images. The bounding boxes predicted by an object detector are shown in green. These images are taken from the SPARK2 [57] dataset, and show the Proba-2 spacecraft class.

be particularly detrimental in resource-constrained scenarios such as those encountered in space. Faster R-CNN [59] and Mask R-CNN [60] are the commonly used multi-stage object detectors for spacecraft localisation.

Single-stage object detectors: These detectors, on the other hand, are lightweight detectors with a reduced number of parameters and have lower latency for real-time detection. YOLO [61] (and its derivatives), SSD [62], and MobileDet [63] are the single-stage detectors applied in the different spacecraft pose estimation algorithms reviewed this survey.

Several other object detectors have also been proposed in the wider computer vision literature, which can be applied for spacecraft localisation. Zaidi *et al.* [64] and Zou *et al.* [65] presented detailed surveys on different classes of object detectors and their characteristics. The modular nature of the hybrid approaches makes it easier to replace object detectors

in the pose estimation algorithms based on criteria such as the number of parameters, resource utilisation, latency and real-time inference.

2) *Keypoint Prediction*: In this stage, the 2D projections of a set of predefined 3D keypoints are predicted from the cropped regions containing the spacecraft using a DL model (see Figure 5). The 3D keypoints are generally defined by the CAD model of the spacecraft. If the CAD model is not available, multiview triangulation (as in [66] [67] [27]) or Structure from Motion (SfM) techniques [68] can be used for reconstructing a wireframe 3D model of the spacecraft containing the 3D keypoints.

Regression of keypoint locations: A common method for predicting keypoints is to directly regress the keypoint locations. Huan et al. [24] uses a CNN regression model with an HRNet [69] backbone for directly regressing the 2D keypoint locations as a $1 \times 1 \times 2M$ vector, where M is the number of keypoints. Park et al. [34] uses a YOLOv2 [70] based architecture with a MobileNetv2 [71] backbone with only 5.64M parameters for regressing keypoints. The lightweight nature of the model makes it suitable for deployment in space hardware or edge devices. Similarly, Lotti et al. [31] also propose a deployable CNN regression model for keypoint regression with EfficientNet-Lite backbone [72], which is obtained by removing operations not well supported for mobile applications (deployment) from the original EfficientNets [73].

Segmentation-driven approach: Algorithms in [35], [36] and [37] follow the segmentation-driven approach from Hu et al. [74] for regressing the keypoint locations, with a dual-headed (segmentation and regression) network architecture and a shared backbone. The input image is divided into a grid and the segmentation head separates the foreground grid cells (containing the spacecraft) from the background. The regression head predicts the location of each keypoint as an offset from the centre of each of the grid cells. Only the predictions from foreground (spacecraft) grid cells contribute to the prediction of the keypoint location, making predictions more accurate. Additionally, [37] also presents different variants of the keypoint prediction model with a lower number of parameters making it suitable for deployment in space hardware. The model with the lowest number of parameters achieving sufficient keypoint prediction accuracy uses a MobileNetv3 [75] backbone that has only 7.8M parameters.

Heatmap prediction: Another method for keypoint prediction is to regress the heatmaps encoding probability of the keypoint locations. The pixel coordinates are then obtained by extracting locations with the highest probability from these heatmaps [23] [25] [27] [28] [30]. The ground truth heatmaps are generated as 2D normal distributions with means equal to the ground truth keypoint locations and unit standard deviations. HRNet [69] network architecture and its derivative, the HigherHRNet [76], is used extensively for heatmap predictions in different algorithms. HRNet architectures maintain high-resolution feature maps throughout the network making it suitable for heatmap prediction tasks. UNet [77] architecture is also used for predicting keypoint heatmaps [30] (see Fig-

ure 7-A). Originally developed for image segmentation, UNet architecture consists of a sequence of downsampling layers (contracting path) that captures relevant semantic information. This is followed by symmetrical upsampling layers (expanding path) for precise location predictions. The use of skip connections in the architecture preserves spatial information during downsampling and subsequent upsampling. Huo et al. [27] presented a lightweight hybrid architecture for keypoint prediction combining a YOLO-like CNN spacecraft detector with a heatmap regression subnetwork (see Figure 7-B). Sharing the backbone network architecture between the object detection and the keypoint prediction brings down the total number of parameters to $\sim 0.89M$, making it suitable to deploy in resource-constrained space systems.

Bounding box prediction: Recently, Li et al. [32] formulated keypoint prediction as a keypoint bounding box detection problem. Instead of predicting the keypoint locations or heatmaps, the enclosing bounding boxes over the keypoints are predicted along with the confidence scores. Authors used CSPDarknet [78] CNN backbone with a Feature Pyramid Network (FPN) [79] for multi-scale feature extraction, followed by a detection head for the keypoint bounding box detection (see Figure 7-C). A similar method is also used in [33]. Here, a counterfactual analysis [80] framework is used to generate the FPN, which is then fed to the keypoint detector.

3) *Pose Computation*: The final stage is to compute the spacecraft pose using the 2D keypoints (from the keypoint prediction stage) and the corresponding pre-defined 3D points [81]. One important step in the pose computation process is to remove the wrongly predicted keypoints, referred to as *outliers*, since the Perspective- n -Point (PnP) [82] solvers are sensitive to the presence of outliers. The RANdom SAMple Consensus (RANSAC) [83] algorithm is commonly used for removing outliers. IterativePnP [84] and EPnP [85] are the two solvers extensively used in the different hybrid algorithms. Recently, Legrand et al. [37] replaced the PnP solver with a Multi-Layer Perceptron (MLP) network architecture, the Pose Inference Network (PIN) [86], for regressing the pose from the predicted keypoints. This makes pose computation differentiable and it can be trained with a pose loss function. In the final step, the estimated pose is further refined by optimising a geometrical loss function [87] such as the keypoint reprojection error [23].

B. Direct End-to-end Approaches

In this survey, direct approaches refer to the use of only one DL model in an end-to-end manner for regressing the spacecraft pose directly from the images without relying on intermediate stages. The models are trained using loss functions calculated from the pose error. Unlike hybrid algorithms, the approach does not require any additional information like camera parameters or a 3D model of the spacecraft apart from the ground truth pose labels. The camera parameters are intrinsically learned by the models during the training process.

Phisannupawong *et al.* [45] proposed a GoogLeNet-based [88] CNN architecture for regressing the 7D pose vector

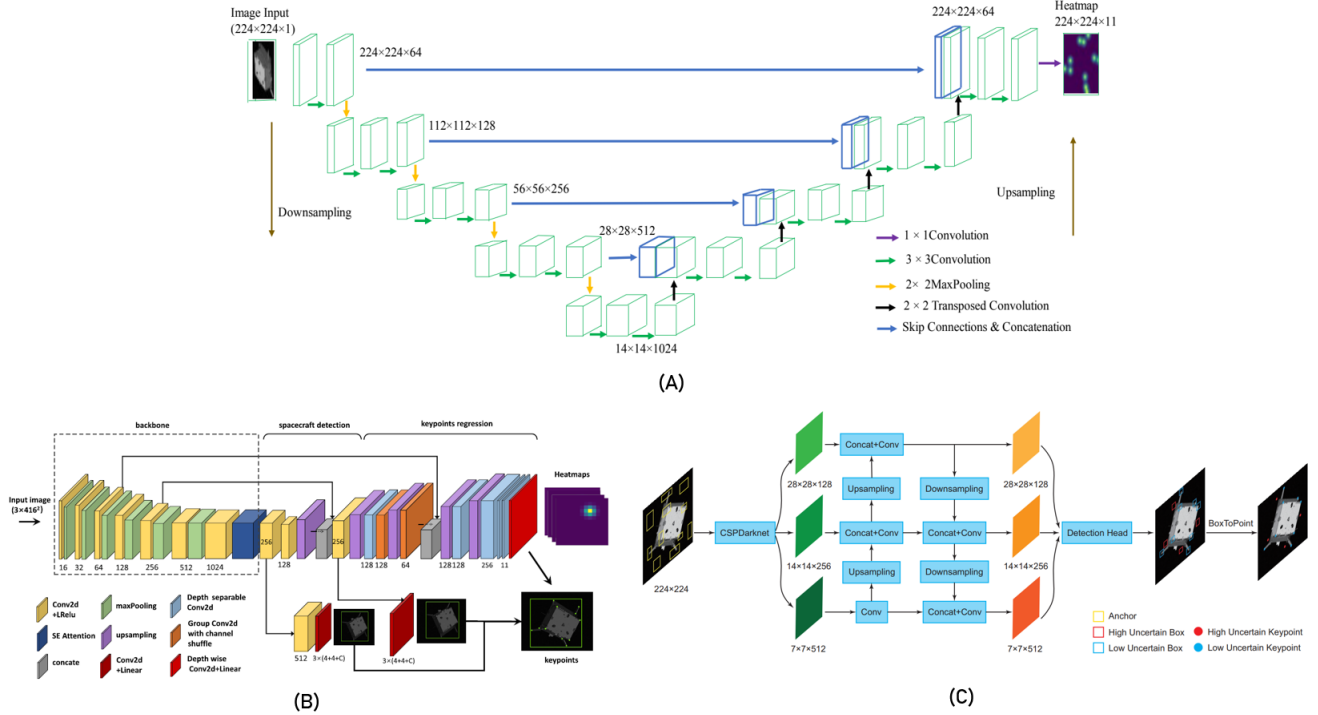


Fig. 7: (A) Keypoint heatmap prediction with a ResNet-UNet architecture [30] (B) YOLO-like CNN detector with a heatmap regression subnetwork [27] (C) Keypoint prediction is formulated as a keypoint bounding box detection problem [32].

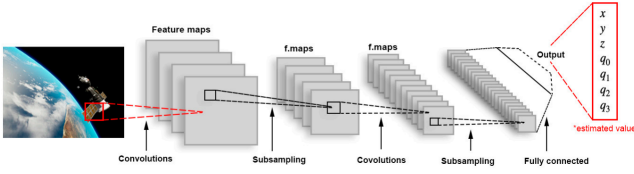


Fig. 8: Network architecture used in [45]. A GoogLeNet [88] based CNN architecture is used to regress the 7D pose vector $[x, y, z, q_0, q_1, q_2, q_3]$.

representing position and orientation quaternion (see Figure 8). The network was trained using different loss functions, an exponential loss function and a weighted Euclidean-based loss function. The experimental results show that the network offers better performance when trained with the latter. However, directly regressing the orientation using a norm-based loss of unit quaternions fails to achieve higher accuracies and results in a larger error margin [41]. This is mainly due to the loss function's inability to represent the actual angular distance of any orientation representation.

Sharma *et al.* [38] proposed discretising the pose space itself into pose classification labels by quantising along four degrees of freedom as illustrated in Figure 9. Two degrees of freedom controlling the position of the camera (w.r.t. to the spacecraft) along the surface of the enclosing sphere, one degree of freedom denoting the rotation of the camera along the bore-sight angle and one degree of freedom determined by the distance of the camera from the spacecraft. An AlexNet-

based [89] CNN network is used for classifying the spacecraft images into these discretised pose label classes, trained with a Softmax loss function [90]. However, this is constrained by the total number of pose class labels to be learned. A larger number of pose labels will need an equivalent number of neurons in the final softmax layer, increasing model size considerably. Also, the method provides an initial guess and requires further refinement to produce more accurate pose estimations.

To overcome these limitations, Sharma *et al.* [39] later presented Spacecraft Pose Network (SPN), a model with a five-layer CNN backbone followed by three different sub-branches (see Figure 10). The first branch localises the spacecraft in the input image and returns the bounding box. The second branch classifies the target orientation in terms of a probability distribution of discrete classes. It minimises a standard cross entropy loss for a set of closest orientation labels. Finally, the third branch takes the candidate orientation class labels obtained from the previous branch and minimises another cross-entropy loss to yield the relative weighting of each orientation class. The final refined attitude is obtained via quaternion averaging with respect to the computed weights, which represents a soft classification approach. The position is then estimated from the constraints imposed by the detected bounding box and the estimated orientation, using the Gauss-Newton optimisation algorithm [91].

Similar network architecture is also used in [44]. A ResNet50 model [92] with a Squeeze-and-Excitation (SE) module [93] is used as the base CNN network for fea-

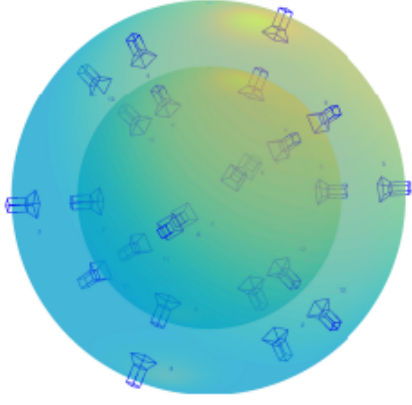


Fig. 9: Illustration of pose space discretisation along four degrees of freedom used in [38]. Two degrees of freedom controlling the position of the camera on the enclosing sphere, one degree of freedom from the rotation of the camera along the bore-sight direction and one degree of freedom from the distance of the camera to the spacecraft.

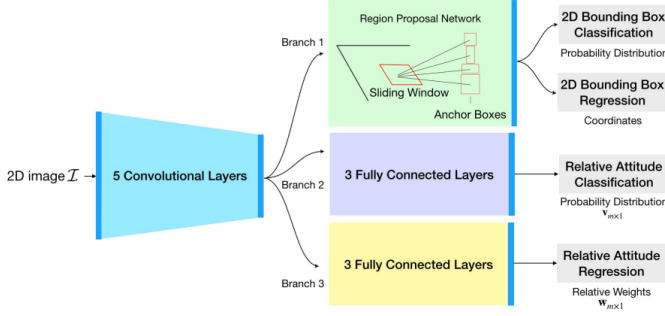


Fig. 10: Network architecture used for spacecraft pose estimation in [39]. Branch 1 localises the spacecraft outputting the bounding box, branch 2 predicts the probability distribution for orientation classification and branch 3 regresses the weights for each orientation class.

ture extraction. The first sub-network, the attitude-prediction-subnetwork, estimates the orientation by soft classification and error quaternion regression. The second pose regression sub-network, predicts the position of the spacecraft by direct regression. Finally, the object detection sub-network detects the spacecraft by predicting the enclosing bounding box. The bounding box is used to validate the position and orientation prediction.

Proença et al. [41] propose URSONet, a ResNet-based backbone architecture followed by two separate branches for the estimation of the position and orientation (see Figure 11). The position estimation was carried out through a simple regression branch with two fully connected layers while minimising the relative error in the loss function. A continuous orientation estimation via classification with soft-assignment coding was proposed for orientation estimation. Each ground truth label is encoded as a Gaussian random variable in

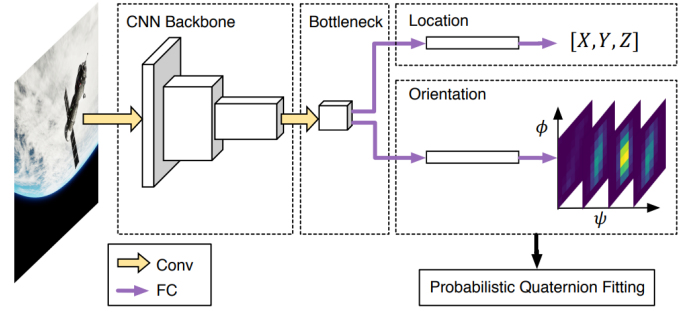


Fig. 11: Direct end-to-end approach for spacecraft pose estimation. The position is regressed directly and the orientation is obtained with soft classification [41]

the orientation discrete output space. The network was then trained to output the probability mass function corresponding to the actual orientation. Poss et al. [42] presented Mobile-URSONet, a mobile-friendly deployable lightweight version of the URSONet. The ResNet backbone was replaced with a MobileNetv2 [71] model, and the number of fully connected layers in the sub-branches was reduced to one (from two). It reduced the number of parameters to a range of 2.2M to 7.4M, 13 times smaller than the URSONet. Moreover, this was achieved without a considerable degradation in performance.

Recently, Park et al. [40] presented SPNv2, improving on the original SPN [39] for addressing the domain gap problem. SPNv2 has a multi-scale multi-task network architecture with a shared feature extractor following the EfficientPose [94] network, which is based on the EfficientDet [95] feature encoder comprised of an EfficientNet [73] backbone and a Bi-directional FPN (BiFPN) [95] for multi-scale feature fusion. This is followed by multiple prediction heads for each of the tasks learned: binary classification of spacecraft presence, bounding box prediction, target position and orientation estimation, keypoint heatmap regression and pixel-wise binary segmentation of the spacecraft foreground. The results show that joint multi-task learning helps in domain generalisation by preventing the shared feature extractor from learning task-specific features. The authors also propose an online domain refinement (ODR) using target domain images (without labels) to be performed on board spacecraft. The ODR fine-tunes SPNv2 on the target images by minimising the Shannon entropy [96] on the segmentation task prediction head. The paper also presents different variants of the algorithm by changing the number of parameters in the EfficientNet backbone. The smallest variant with 3.8M parameters has comparable performance to the best-performing variant with 52.5M parameters on the SPEED+ synthetic dataset.

Garcia et al. [43] presented a network architecture with two CNN modules: the translation and orientation modules, for pose estimation (see Figure 12). The translation module has a UNet architecture [77] for predicting the 3D position $[x, y, z]$ of the target (from the intermediate feature embedding layer) and the 2D spacecraft location in the image $[u, v]$ (from

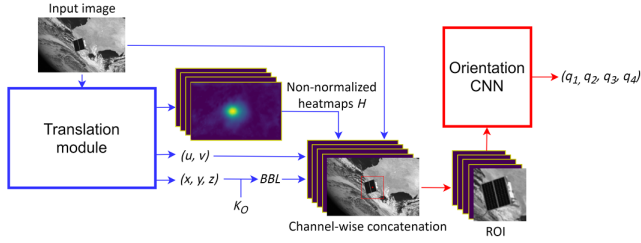


Fig. 12: LSPNet architecture for spacecraft pose estimation [43]

the final heatmap output). This is then used to generate the enclosing bounding box for the spacecraft and the RoI is cropped out. The orientation module with a CNN regression network predicts the spacecraft orientation $[q_0, q_1, q_2, q_3]$ from the cropped RoI.

C. Algorithm Comparison

In this section, different spacecraft pose estimation algorithms are compared. Table I and Table II summarise different hybrid and direct algorithms, respectively, with a comparison of DL models used, the total number of parameters, and the pose accuracy. The performance of the pose estimation algorithm is expressed in terms of the mean position and orientation errors. The position error is calculated as:

$$E_t = \|t_{\text{predicted}} - t_{\text{groundtruth}}\|_2 \quad (1)$$

and the orientation error is calculated as:

$$E_R = 2 * \arccos(|\langle q_{\text{predicted}}, q_{\text{groundtruth}} \rangle|) \quad (2)$$

where, $t_{\text{predicted}}$, $t_{\text{groundtruth}}$ are the predicted and the ground truth translation vectors and $q_{\text{predicted}}$, $q_{\text{groundtruth}}$ are the predicted and the ground truth rotation quaternions respectively. $|\langle, \rangle|$ indicates the absolute value of the vector dot product and $\|_2$ is the Euclidean norm. The mean position and orientation error values on the SPEED [19] synthetic test set are reported where available [19]. In other cases, the error values on the corresponding synthetic published dataset are reported. Similarly, in many instances, authors do not report the total number of parameters in their algorithms. In such cases, an approximate number of parameters is estimated based on the known backbone models and frameworks used. This survey is the first attempt to compare different DL-based spacecraft pose estimation algorithms in terms of performance reported on different datasets and the number of model parameters with available information in the literature.

A key aspect of the spacecraft pose estimation algorithms is the deployment on edge devices for their use in space. Unlike the commonly used resource-abundant workstations, computing resources are scarce in space systems. Hence, deploying large DL models that have a very large number of parameters is difficult. On the other hand, using smaller DL models with a lower number of parameters leads to a drop in performance. Thus, a trade-off is needed between the

use of large, high-performing models and smaller, deployable models. Based on Table I and Table II, Figure 13 shows this trade-off by plotting the algorithm performance against the total number of model parameters. The results show that the algorithms [28], [32], [97] and the SLAB Baseline [34] provide a good trade-off in terms of the performance and the number of parameters.

Another factor of comparison for algorithms is the modular nature of the approaches themselves. The hybrid algorithms are built by integrating three components: spacecraft localisation, keypoint regression and pose computation. This helps to work and improve each stage of the algorithms in isolation. For example, changes in the camera model can be incorporated into the pose computation stage without retraining the localisation and keypoint regression models. This provides more flexibility in building the algorithms for different pose estimation applications. By contrast, the direct algorithms comprise only a single DL model trained end-to-end. The entire model has to be retrained to incorporate changes such as changes in camera parameters.

In terms of performance comparison between the approaches, analysis of the top-10 methods from the first edition of ESA Kelvin Satellite Pose Estimation Challenge (KSPEC'19) [19] show that the hybrid approaches perform comparatively better than the direct approaches. The hybrid and direct algorithms have mean position errors of 0.0083 ± 0.0269 m and 0.0328 ± 0.0430 m and mean orientation errors of $1.31 \pm 2.24^\circ$ and $9.76 \pm 18.51^\circ$, respectively. Analysis of the recently concluded second edition of the same challenge (KSPEC'21) [20] also gives similar indications. Winning algorithms on both streams of the challenge used the hybrid approach.

D. Limitations

Recently, several promising algorithms have been developed for DL-based spacecraft pose estimation using both the hybrid and the direct approaches. However, these algorithms still have several limitations that need to be considered and have room for further improvement. This section highlights these limitations with discussions on each topic.

1) *Deployability*: Deployability is a key aspect of any space algorithm. Despite the recent progress in spacecraft pose estimation algorithm development, the deployment remains an important open research question. The limitations of current algorithms in terms of deployability refer to the challenges of implementing these algorithms in real-world space missions.

Among the current research works, only a small fraction of the developed algorithms are tested and evaluated on edge systems for space deployment [30], [33], [97]. Also, authors rarely report factors effecting algorithm deployability such as latency, inference time, memory requirements, power consumption and computational cost. These missing details are important to understand the deployability of a model [98], [99], on resource-constrained environment such in a space system with limited computational capabilities.

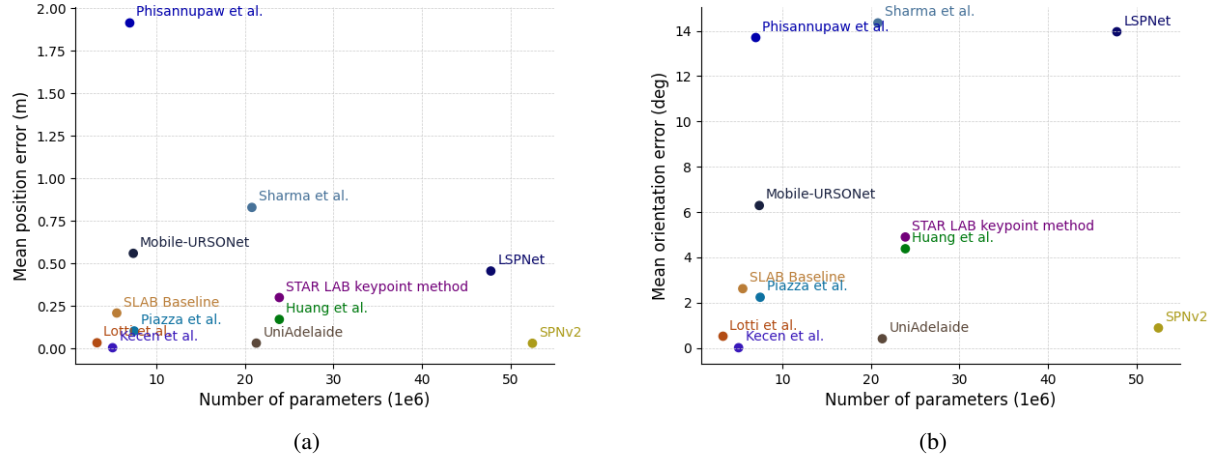


Fig. 13: Comparison of pose estimation algorithms in terms of number of parameters versus (a) position error and (b) orientation error.

Another limitation is the extensive use of off-the-shelf DL models and frameworks (refer to Table I and Table II). While these off-the-shelf models work well on a workstation, they may not be suitable for space deployment due to several reasons. Primarily, these models are designed to work on systems with abundant resources and are computationally expensive, requiring significant processing power and memory. Secondly, these models (or certain DL layers) may not be supported [100] by the AI accelerators used in current space systems like FPGA-based [101], [102] accelerators. Hence it is required to build algorithms with architectures specifically customised for space applications and hardware.

2) *Explainability*: Explainability refers to the ability to understand how an algorithm arrives at its predictions, and it is an essential factor in building trust and ensuring safety in critical applications such as space missions. This makes error analysis and troubleshooting easier. A key limitation of the current DL-based spacecraft pose estimation algorithms is their lack of explainability. In the direct approach, the black-box nature of DL models in general [103] makes interpreting the errors and failures very difficult. Comparably, the hybrid approach tackles the spacecraft pose estimation problem in stages, providing better interpretability. However, these algorithms still lack capabilities such as reasoning [104] or modelling the uncertainty between the input data and the predictions made [105].

3) *Robustness to Illumination Conditions*: Monocular vision-based algorithms are in general sensitive to changes in lighting conditions. This can affect the accuracy and robustness of the pose estimation, especially in the dynamic illumination conditions in space. For example, shadows, reflections and sun glare can all create visual noise and make it difficult to identify and track features on the spacecraft. Analysis of the results (see Figure 14) from the latest edition of KSPEC (KSPEC'21) [20] shows that even the best vision-

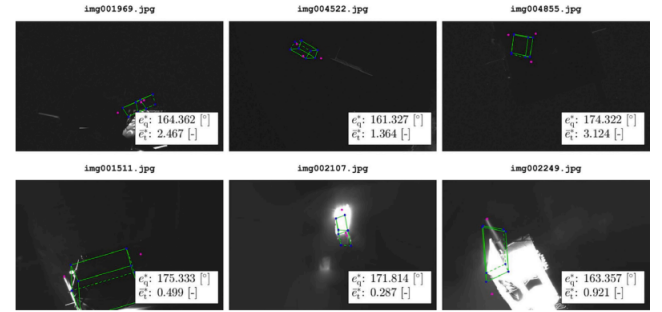


Fig. 14: Visualization of the worst 3 predictions made by stream-1 winning method of the KSPEC'21 challenge on *lightbox* (top-row) and *sunlamp* (bottom-row) images [20]. These results show considerable drop in accuracy of estimated poses (shown in green) under extreme lighting conditions, highlighting a important limitation of vision-based spacecraft pose estimation algorithms.

based spacecraft pose estimation algorithms performs poorly on images with extreme lighting conditions.

Overcoming these limitations will require continued research and development in areas including algorithm design, evaluation protocols on edge devices, sensor technology and modelling of environmental factors. Section IV outlines future directions of research in spacecraft pose estimation algorithm development to address these challenges. Finally, any DL-based algorithm development cannot be separated from the question of the datasets, both for training and validating the algorithms. The next section (Section III) presents a detailed discussion of spacecraft pose estimation datasets (Section III-A) with a focus on the domain gap problem (Section III-B) and a discussion on their limitations (Section III-C).

TABLE I: Summary of the hybrid algorithms for spacecraft pose estimation. Details of the object detector and keypoint prediction models (including the estimated number of parameters) and the pose computation methods used are provided. The mean position and orientation error values on the SPEED synthetic test set are reported where available. In cases where the number of parameters is not reported by the authors, estimated values based on the known backbone models and frameworks are given.

Ref	Object Detector	Parameters (millions)	Keypoint Prediction	Parameters (millions)	Total Parameters (millions)	Pose Computation	Mean position error (E_t) (m)	Mean orientation error (E_R) (deg)
UniAdelaide [23]	Faster-RCNN [59] with HRNet-W18-C [69] as the backbone	~21.3* [106]	Pose-HRNet-W32 [107]	~28.5 [107]	~49.8 (176.2 [31])	PnP + RANSAC refined with a geometric loss optimized using SA-LMPE optimiser	0.0320 ⁺	0.4100 ⁺
EPFL_cvlab [35]	Not applied	-NA-	Yolov3 [108] with DarkNet-53 [108] as the backbone followed by a segmentation and regression decoder branches	~59.1 [109]	~59.1 (89.2 [31])	EPnP [85] + RANSAC	0.0730 ⁺	0.9100 ⁺
SLAB Baseline [34]	YOLOv3 [108] with MobileNetV2 [71] as the backbone	5.53	YOLOv2 [70] with MobileNetV2 [71] as the backbone	5.64	11.2	EPnP	0.2090 ⁺	2.6200 ⁺
Huo et al. [27]	Tiny-YOLOv3 [108] architecture** with a detection subnetwork	-NA-	Tiny-YOLOv3 [108] architecture** with a regression subnetwork	-NA-	~0.89	PnP+RANSAC refined with a Log-cosh geometric loss optimized by Levenberg-Marquardt solver [110]	0.0320	0.6812
Piazza et al. [28]	YOLOv5	7.5	HRNet32 [107]	~28.6* [76]	~36.1	EPnP refined with a geometric loss optimised by Levenberg-Marquardt solver	0.1036	2.2400
Huan et al. [24]	Cascade Mask R-CNN [111] with HRNet as backbone	-NA-	HRNet [107]	~28.5 to ~63.6 [107]	-NA-	EPnP refined with a Huber style geometric loss optimised as non-linear least-squares problem	0.1823	2.8723

STAR LAB keypoint method [25]	Faster-RCNN [59] with ResNet50 [92] backbone	~23.9* [112]	HigherHRNet [76] with HRNet- W32 [107] as the backbone	~28.6* [76]	~54.2	PnP + RANSAC	0.3000 (URSO- OrViS dataset)	4.9000 (URSO- OrViS dataset)
Black et al. [29]	SSD [62] MobileNetV2 [71]	-NA-	MobilePose [113] architecture with MobileNetV2 [71] as backbone	-NA-	6.9	EPnP + RANSAC	1.0800 (Cygnus dataset)	6.4500 (Cygnus dataset)
Wide-Depth- Range [36]	Not applied	-NA-	FPN [79] architecture with DarkNet- 53 [108] as the backbone	51.5	51.5	PnP + RANAC with and without a pose refinement strategy	-NA-	-NA-
Cosmas et al. [30]†	YOLOv3 [108]	~59.1* [114]	ResNet34- UNet [77], [92] architecture	~21.5* [115]	~80.6	-NA-	-NA-	-NA-
Lotti et al. [31]†	MobileDet [63]	3.3	Regression head with an EfficientNet- Lite [73] backbone	-NA-	15.4	EPnP + RANSAC optimised by Levenberg- Marquardt solver	0.0340	0.5200
Kecen et al. [32]†	YOLOX-Tiny [116]	~5.06 [116]	FPN [79] archi- tecture with CSP- Darknet53 [78] as the backbone	~27.6 [78]	~32.66	EPnP	0.0049	0.0129
CA- SpaceNet [33]	Not used	-NA-	Keypoint prediction head having three FPNs [79] with two DarkNet- 53 [108] networks as the backbones	-NA-	51.29 M †	PnP	-NA-	-NA-
Legrand et al. [37]†	An ideal object detec- tor assumed	-NA-	DarkNet-53 [108] pre-trained on Linemod [117] with two decoding heads - a segmentation head and a regression head	71.2	-NA-	PIN architec- ture [86] consists of an MLP that aggregates local features per keypoint into a single representation.	0.201	4.687

* Results from KSPEC first edition [19]

**Backbone shared between the object detector and the keypoint prediction model

†Best performing variant considered

TABLE II: Summary of direct end-to-end algorithms for spacecraft pose estimation. Details of the network architectures used, along with an estimated number of parameters, are presented. The error values on the SPEED synthetic test set are reported where available. In cases, the number of parameters is not reported by the authors, an estimated number of parameters based on the backbone models used are given.

Reference	Model architecture	Parameters (millions)	Mean position error (E_t) (m)	Mean rotation error (E_R) (deg)
Sharma et al. [38]†	AlexNet [89] with half as many kernels per layer as the original AlexNet architecture, with the last fully connected layer containing as many neurons as the number of pose labels	~20.8	0.83 (Imitation-25 dataset)	14.35 (Imitation-25 dataset)
SPN [39]	A 5-layer CNN with 3 sub-branches for bounding box classification and regression, relative orientation classification and relative orientation weights regression.	-NA-	0.7832	8.4254
SPNv2 [40]†	Bi-directional Feature Pyramid Network (BiFPN) [95] with EfficientNet [73] backbone and with multi-task head networks shared by the features at all scales.	52.5	0.031 (SPEED+)	0.885 (SPEED+)
URSONet [41]	ResNet18, ResNet34, ResNet50, ResNet101 [92] base networks with 2 sub-branch networks for position regression and probabilistic orientation estimation via soft classification.	~11.4 to ~42.8 [112] (~500**)	0.1450 ⁺	2.4900 ⁺
Mobile-URSONet [42]†	MobileNet-v2 [71] based network, pre-trained on ImageNet [118], with 2 sub-branches for position regression and probabilistic orientation estimation via soft classification.	7.4	0.5600	6.2900
LSPnet [43]	ResNet50 [92] base architecture for position regression followed by an up-sampling CNN for object localisation and a second ResNet50 for orientation regression.	~47.8 [112]	0.4560	13.9600
Huang et al. [44]	ResNet50 [92] base network with 3 sub-branch networks for object detection, position regression and orientating soft classification.	~23.9 [112]	0.1715 (URSO-OrViS dataset)	4.3820 (URSO-OrViS dataset)
Phisannupawong et al. [45]	A modified version of GoogLeNet [88] that forms a general pose estimation model as implemented in PoseNet [119]. The softmax classifiers in the original GoogLeNet were replaced with affine regressors and each fully connected layer was modified to output a 7D pose vector.	~7.0	1.1915 [#] (URSO-OrViS dataset)	13.7043 [#] (URSO-OrViS dataset)

†Details of the best performing variant reported

⁺Results from KSPEC first edition [19].

^{**}Number of parameters in the best performing ensemble of models reported by the authors

[#]Median values reported

III. DATASETS

The use of DL models in spacecraft pose estimation necessitates proper training to achieve the robust performance demanded by space applications. The quality of the datasets is likely equally influential in DL model performance compared to designing an effective DL algorithm to reach the intended performance. Large datasets [122], [123] with a wide range of application scenarios are usually considered to train DL models, which helps them generalise well for unseen scenarios. Though DL algorithms are evolving towards few-shot [124] and zero-shot [125] learning, solving 6 DoF pose prediction problems with high accuracy still depends on large datasets with images spanning a wide range of scenarios [126], [127].

Currently, there is a lack of publicly available space-borne image datasets. This limits the application of DL models and their validation to specific targets where actual space-borne images are available and to a limited range of operation scenarios. To overcome this limitation, image rendering tools are the preferred way to generate realistic space-borne images and testbeds are considered for on-ground validation. The rendering tools help generate thousands of images for a wide range of targets with annotations for any user-defined applications such as object detection, semantic segmentation and 6 DoF pose estimation. These generation tools also provide a lot of flexibility to adapt parameters such as camera models, orbital lighting conditions, etc., depending on the final use-case application.

Spacecraft pose estimation algorithms are usually part of vision-based navigation systems and are validated in a dedicated testbed facility that can simulate the orbital relative motion using robotic arms [128], [129] or air-bearing [130] platforms under realistic space lighting conditions. The target mock-up used in such facilities will be scaled or original depending on various factors, including the size of the facility, mock-up size, application scenario, etc. While synthetic imagery can be mass-produced to address any requirements, the images produced from testbed scenarios are limited to a certain extent. It includes the Earth in the background, the accurate position of the sun, earth's albedo; such characteristics differentiate the lab/testbed imagery from the actual space imagery.

From the above discussion, it is evident that the spacecraft pose estimation deals with images from three domains (i.e., synthetic, lab and actual space imagery) during the development, testing/validation and deployment phases. It is the nature of the DL models to overfit the model to the features specific to the training domain, and this challenge is well-known in the literature as *domain gap* [131], [132] problem. So, the algorithms need to consider the aspect of domain generalisation from the data viewpoint to improve the algorithm's performance.

A. Summary of Datasets, Simulators and Testbeds

This section provides a summary of the spacecraft pose estimation datasets, simulators and rendering tools for synthetic image generation, and testbeds for validation.

Datasets: Table III summarises the properties of the major spacecraft pose estimation datasets. The properties of the datasets include the number of images, the target spacecraft model, image resolution, annotations and the rendering tools used for the synthetic image generation. The number of images in the currently available spacecraft pose estimation datasets is between 10^4 and 10^5 . This is relatively low compared to some typical datasets used for other machine learning tasks such as image classification and object detection. The COCO [133] dataset, one of the standard datasets used for object detection, contains ~300k images. ImageNet dataset [118] primarily used for classification contains ~14M images. Similarly, YCB dataset [127], a recent generic dataset for 6 DoF pose estimation, has ~133k images.

The target spacecraft model used in the datasets also plays a vital role in determining the dataset characteristics. For example, a smaller target size will lead to a smaller operation range and vice-versa. The TANGO satellite [134] model used in the multiple datasets [19], [34], [34], [38], [120], [121] has a coarse dimension of 80×75×32cm will lead to the operation range of ~10m. However, for Soyuz or Cygnus models in other datasets increases the operating range to 40 ~ 80 m. Similar constraints will apply to testbed data as well. A 1:1 mockup scale of TANGO spacecraft in SPEED+ [121] leads to a lower range in the lab-generated images due to the size constraint of the facility. Usually, a scaled mock-up is considered a solution to increase the validation range in the testbed scenarios.

The level of annotations may vary for different datasets; for spacecraft pose estimation applications, each image in the dataset must be appropriately annotated with corresponding relative 6DoF pose labels. All the datasets mentioned in Table III are adequately annotated with 6DoF pose labels. However, the hybrid algorithm approach discussed in Section II-A demands secondary annotations such as the bounding boxes and the keypoints. To recover the secondary annotations from pose labels, it is necessary to have 3D information on the edges or vertices of the target. Even for the standard datasets such as SPEED [19] and SPEED+ [121], the only way to use a hybrid approach is to recover the 3D locations of interested keypoints is via the 3D reconstruction methods [23]. These recovered keypoints will be used to construct secondary annotations such as bounding boxes, keypoints, segmentation masks and even ellipse heatmap annotations [135]. The lack of secondary annotations can be an issue for multi-task learning approaches where the annotations (such as segmentation masks) could be used to define auxiliary tasks intended to prevent learning domain-specific features to improve generalisation [40]. Several learning-based approaches are evolving to generate secondary annotation to address the label scarcity, such as depth estimation using a single image depth estimator [136] and an image segmentation technique [137]. Some self-supervised approaches are evolving as an alternate way to get bounding box annotations for a single target in the image [138]. Though these approaches aid annotations, they cannot replace the properly calibrated annotations recorded during synthetic data generation.

Dataset	Year	Syn/Lab/Space	Spacecraft	Resolution	I	Range	Tools	Public
SHIRT [120]	2022	5k/5k/-	Tango	1920x1200	G	$\leq 8\text{m}$	OpenGL	✓
SPARK2-Stream2 [57]	2022	30k / 900 / -	Proba-2	1440 x 1080	C	[1.5m,10m]	Blender	✓
COSMO [97]	2022	15k / - / -	COSMO-SkyMed	1920 x 1200	C	[36m,70m]	Blender	✓
SwissCube [36]	2021	50k / - / -	SwissCube	1024 x 1024	C	[0.1m, 1m]	Mitsuba 2	✓
SPEED+ [121]	2021	60k / 10k / -	Tango	1920 x 1200	G	$\leq 10\text{m}$	OpenGL	✓
Cygnus [29]	2021	20k / - / 540	Cygnus	1024 x 1024	C	[35m,75m]	Blender	✗
SPEED [19]	2020	15k / 305 / -	Tango	1920 x 1200	G	[3m,40.5m]	OpenGL	✓
URSO [41]	2019	15k / - / -	Dragon, Soyuz	1080 x 960	C	[10m,40m]	Unreal Engine 4	✓
PRISMA12K [34]	2019	12k / - / -	Tango	752 x 580	G	-	OpenGL	✗
PRISMA12K-TR [34]	2019	12k / - / -	Tango	752 x 580	G	-	OpenGL	✗
Sharma et. al. [38]	2018	500k / - / -	Tango	227 x 227	C	[3m,12m]	OpenGL	✗

TABLE III: Review of recent spacecraft pose estimation datasets, sorted by year. The *Syn/Lab/Space* column is, the number of synthetic, lab and space-borne images in the dataset, respectively. The *Spacecraft* column specifies the spacecraft used in the dataset. The *resolution* column corresponds to the width x height of the images, in pixels. The *I* column indicates if the images are RGB (C) or grey-scale (G). The *Range* column indicates the distance between the camera and the spacecraft. The *Tools* column is a list of the rendering software used to generate the synthetic data. Finally, the *Public* column indicates the availability of the dataset to the public. The links to the publicly available datasets are included in Appendix VI-B.

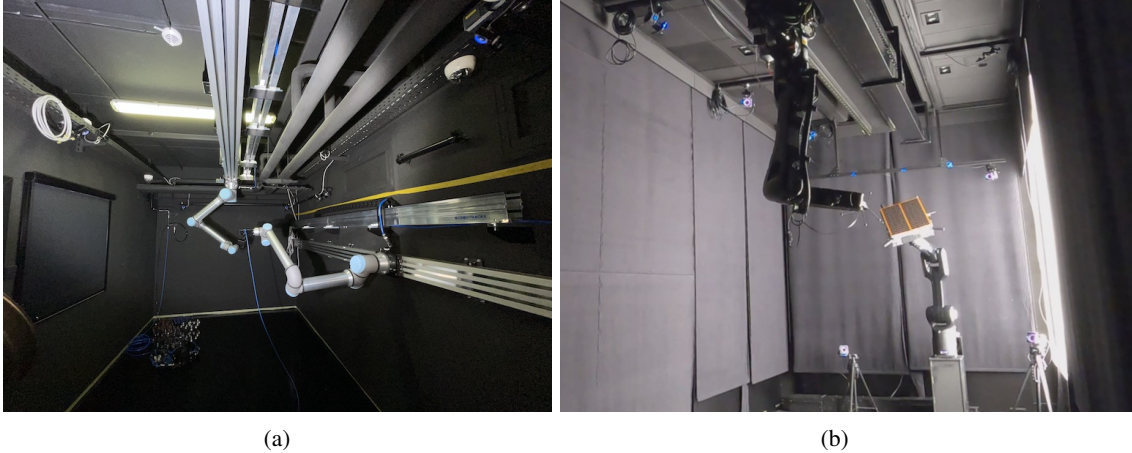


Fig. 15: (a) SnT Zero-G Lab at the University of Luxembourg [128] (b) TRON facility at Stanford University [129]

Simulators and Rendering Tools: Computer graphics allow us to create realistic images of objects based on high-quality textures using ray tracing. Ray Tracing techniques mimic how light interacts with the real world and rely on evaluating and simulating the path of view lines from the observer camera to objects in the field of view. This simulation enables the calculation of the light intensity of associated pixels. Several efforts were made towards creating simulators for space applications. Realistic image simulation tools were used in previous missions to aid vision-based navigation in space/planetary environments (such as the Lunar environment, Asteroid surface), and it includes the PANGU (Planet and Asteroid Natural scene Generation Utility) [139] and the SurRender [140] by Airbus. The University of Dundee has developed the PANGU simulation tool, which generates realistic, high-quality, synthetic surface images of planets and asteroids.

PANGU uses a custom GPU-based renderer to render the scene. Airbus’s Surrender can be used in two modes of image rendering, ray tracing and OpenGL [141]. It can produce physically accurate images providing the known irradiance (each pixel contains an irradiance value expressed in W/m²). Other general rendering tools such as Blender [97], Unreal Engine [41], and Mitsuba [36] were also used to generate synthetic images. The main issue with these tools is that they are designed for general usage and are not customised for space imagery. A brief comparison of rendering tools for synthetic imagery was provided in [142]. Recently, efforts [19], [143] have been made toward developing simulation tools specific for the purpose of synthetic image generation for spacecraft pose estimation. SPEED and SPEED+ images are obtained using the Optical Simulator [144], based on an OpenGL rendering pipeline. The images from SPEED and SPEED+

are validated against the real images of TANGO spacecraft from the PRISMA mission using histogram comparison [19]. However, to our knowledge, no tool can be considered a de facto standard to generate space imagery for spacecraft pose estimation.

Testbeds: In spacecraft pose estimation, collecting images from space for training and evaluating algorithms is extremely difficult and expensive. Laboratory testbeds (see Figure 15) are considered as an alternative to replicate relative motion and orbital lighting conditions. Table IV, summarises different laboratory testbed facilities based on their size, manipulation capabilities, tracking systems, perception sensors and orbital motion simulations. Some of the SoTA testbed includes The Robotic Testbed for Rendezvous and Optical Navigation (TRON) at Stanford’s Space Rendezvous Laboratory (SLAB) [129], STAR Lab at the University of Surrey [142], SnT Zero-G Lab at the University of Luxembourg [128], GMV Platform-Art [145], [146], German Aerospace Center European Proximity Operations Simulator 2.0 (DLR EPOS) [147] and European Space Agency’s GNC Rendezvous, Approach and Landing Simulator (GRALS) [148]. These testbeds generally have robotic manipulators to carry the payloads. The payloads can be different target spacecraft mock-up models or mounted cameras mimicking a chaser. Different lighting equipment has been used for simulating space conditions. For instance, in SPEED+ [121], the images collected in a sunlamp setup replicate the sun’s bright light, and those collected with a lightbox setup emulate the diffused light of the earth’s albedo, respectively. Motion capture systems are extensively used to collect pose labels based on the reflective markers attached to the target and cameras. However, these motion capture systems should be carefully calibrated [129] to generate accurate ground truth data, which can be tedious and time-consuming.

The next section discusses the major issue with the current spacecraft pose estimation datasets: the domain gap between synthetic data used for training and the real laboratory/ spaceborne images used for testing/ validating and deploying the DL-based algorithms.

B. Bridging the Domain Gap

Any DL-based algorithm trained on a synthetic dataset is likely to suffer from a performance drop when tested on real images (whether acquired within a ground-based laboratory or in space), which is referred to as the *domain gap* [150] problem. Following the related computer vision terminology, the training dataset arises from a *source* domain while the test dataset belongs to the *target* domain. More subtly, a domain gap persists even when the real source and target datasets are acquired under different (laboratory and space) environmental conditions [151]. To ensure the reliable performance of DL-based spacecraft pose estimation algorithms in real-world space missions, it is, therefore, crucial to bridge the domain gap. Several methods have been used in spacecraft pose estimation literature for this purpose. These methods are classified into two categories:

- Data level methods: Expanding or adding diversity to the training data by applying different techniques to alter the images, such as 1) *data augmentation* [40] or 2) *domain randomization* [34]
- Algorithm level methods: Adapting the learning procedure of the model by using different techniques, such as 3) *multi-task learning* [152] or 4) *adversarial learning* [121], to make the features extracted from images as less domain-dependent as possible

1) *Data Augmentation:* This involves artificially creating additional training data by applying various transformations to the existing data [153]. This is done to increase the size and variations of the training set and to make the model more robust to unseen variations in the input data, i.e. to improve the generalisation to unseen domains. Data augmentation techniques used in spacecraft pose estimation algorithms can be further categorised into:

- Pixel-wise data augmentations such as blurring, noising or changing the image contrast
- Spatial-level data augmentations such as rotation or scaling

The main difference between the two categories is their effect on the pose labels. The pixel-level augmentations only affect the input image, whereas the spatial-level augmentations require modifying both the input image as well as the pose label, which can be difficult. Figure 16 illustrates different data augmentation techniques (pixel and spatial-level) applied to a reference image of PROBA-2 spacecraft from the SPARK2 [57] dataset. Finally, even though data augmentation generally helps with the domain gap problem, there can be instances when applying data augmentation can be counter-productive. For example, the Random Erase augmentation used by Park et.al [40] is shown to cause a drop in the pose estimation performance. Consequently, finding the best set of augmentations for a given context is a hard task in itself [154]. Table V provides a summary of data augmentation methods used in spacecraft pose estimation algorithms surveyed in this paper.

2) *Domain Randomization:* The goal is to help the model generalise by training it on a set of sufficiently randomized source data so that the target domain appears as just another randomization to the model [155]. Hence, the expectation is that the model will be less prone to the domain gap [156]. An example of domain randomization in the context of spacecraft pose estimation is provided in [34], where the spacecraft texture is randomized using the Neural Style Transfer (NST) technique presented in [157]. Domain randomization can be seen as a particular case of data augmentation: one does not search for a set of augmentations relevant to a context, but for a sufficiently varied set of augmentations that will make the actual scene appear as just another variation.

3) *Multi-Task Learning:* In this approach, a single DL model is trained to perform multiple related tasks (a primary task and several secondary/ auxiliary tasks) simultaneously. The assumption here is that the model will generalise better on the primary task (spacecraft pose estimation in this context)

TABLE IV: Summary of different laboratory testbed facilities for evaluating spacecraft pose estimation algorithms

Facility	STAR Lab [142]	TRON [129]	SnT Lab [128]	Zero-G	GMV Platform-Art® [145] [146]	DLR EPOS 2.0 [147]	GRALS [148]
Illumination	<ul style="list-style-type: none"> Forza 500 LED spotlight 	<ul style="list-style-type: none"> LED panels (for diffused light) Metal-halide arc lamp (for sunlight) 	<ul style="list-style-type: none"> Godox SL-60 LED Video Light Aputure LS 600d Pro 		<ul style="list-style-type: none"> Numerically controlled Sun emulator 	<ul style="list-style-type: none"> Osram ARRI Max 12/18 (with a 12 kW hydrargyrum medium-arc iodide lamp) 	<ul style="list-style-type: none"> Dimmable, uniform and collimated light source
Perception Sensor	<ul style="list-style-type: none"> FLIR Blackfly (monocular camera) 2D/3D LIDAR Intel RealSense D435i (RGBD camera) 	<ul style="list-style-type: none"> Point Grey Grasshopper 3 (monocular camera) 	<ul style="list-style-type: none"> FLIR Blackfly (monocular camera) Prophesee EKV4 (event camera) Intel RealSense D435i (RGBD camera) 		<ul style="list-style-type: none"> Optical navigation camera Industrial laser sensor A set of GPS-like pseudolites 	<ul style="list-style-type: none"> Prosilica GC-655M (CCD camera) PMDtec Camcube 3.0 (PMD camera) Bluetechnix Argos3D-IRS1020 DLR Prototype (PMD LiDAR) 	<ul style="list-style-type: none"> Prosilica GC2450 (monocular camera)
Manipulator (Robotic Arms)	<ul style="list-style-type: none"> UR5 	<ul style="list-style-type: none"> KUKA 	<ul style="list-style-type: none"> UR10e 		<ul style="list-style-type: none"> Mitsubishi PA10-6CE KUKA KR150-2 	<ul style="list-style-type: none"> KUKA KR100HA KUKA KR240-2 	<ul style="list-style-type: none"> KUKA UR5
Tracking System	Qualisys	Vicon	OptiTrack		Model-based tracking algorithm based on virtual visual servoing & Kanade-Lucas-Tomasi (KLT) feature tracker algorithm	Vision Based Navigation Sensor System (VIBANASS)	VICON
Background Material	Black background curtains	Light-absorbing black commando curtains	Blind made of non-reflective black textile from inside and outside		Black curtains fully covering the walls and ceiling	Black curtain and a black wrapping of one of the robots made of Molton material	Black background curtains
Simulated Operations	<ul style="list-style-type: none"> Proximity 	<ul style="list-style-type: none"> Rendezvous Proximity 	<ul style="list-style-type: none"> Proximity Rendezvous Orbital maintenance operations 		<ul style="list-style-type: none"> Rendezvous Proximity 	<ul style="list-style-type: none"> Rendezvous Docking/berthing Proximity 	<ul style="list-style-type: none"> Rendezvous Proximity
Dimensions (WxLxH)	3m×2m×2.5m	8m×3m×3m (simulation room) and 6m (track)	5m×3m×2.3m		15m	25m (track)	4m
ROS [149] Supported	Yes	-NA-	Yes		No	No	No

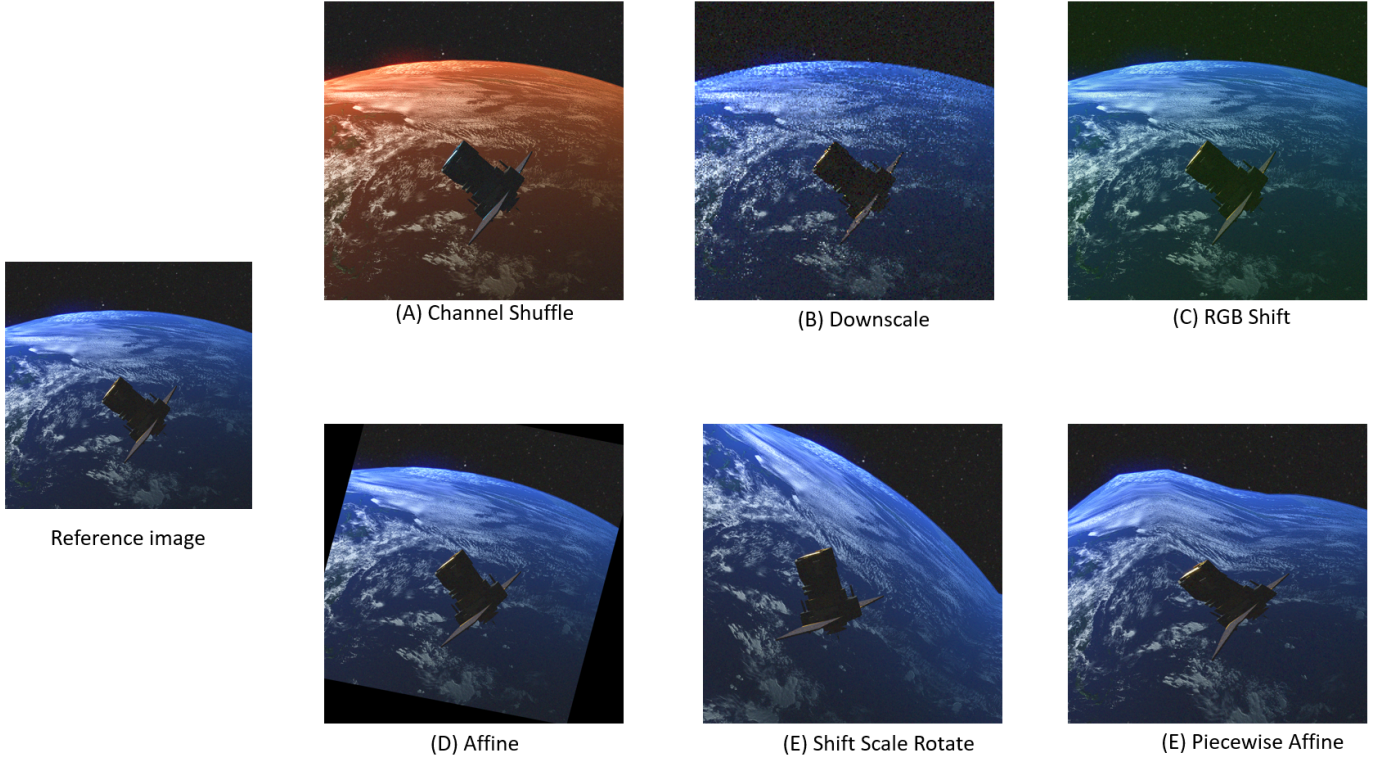


Fig. 16: Illustration of different data augmentation methods used on the same reference image taken from SPARK2 [57] dataset. Images A, B and C show examples of pixel-wise augmentation methods and images D, E and F show the application of spatial augmentation methods. The captions refer to the corresponding functions used by the Albumentations Python library.

by being less prone to the noise induced by the primary task [158]. The most common way of implementing multi-task learning is to have a shared backbone architecture extracting features and feeding these features to the task-specific layers [40] (see Figure 17). Here EfficientPose [94] network architecture is modified with the addition of two heads: one for the segmentation of the spacecraft and one to compute the 2D heatmaps associated with pre-designated keypoints on the spacecraft. The results show that when the model is trained with different head configurations, the best performance is reached when all the task heads are enabled, thereby showing the effectiveness of multi-task learning. However, the authors show that all the heads do not contribute to the same extent; the segmentation head only improves the performance slightly. This highlights one of the key challenges in multi-task learning: identifying the correct set of secondary tasks that is relevant for a particular primary task [159].

4) *Domain-Adversarial Learning*: This technique [160] is applied to spacecraft pose estimation [121] to bridge the domain gap. The goal here is to help the model learn features that are domain-invariant but discriminative with respect to the pose estimation task. A domain classifier, whose purpose is to discriminate between the source and the target domain, is attached to the model and its loss function maximised over the learning phase. The underlying idea of this method is that the less this classifier can distinguish between the source and the

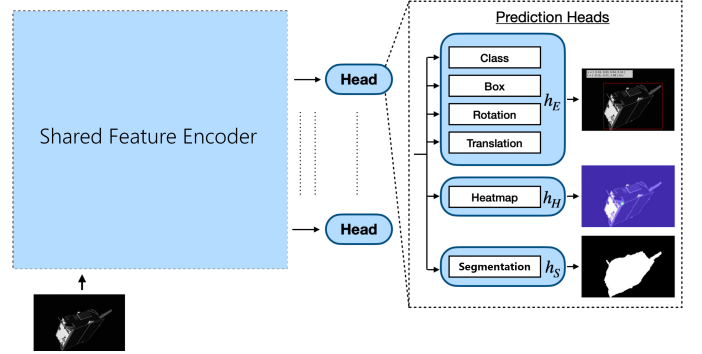


Fig. 17: A model architecture used for multi-task learning, where some layers are shared between all tasks, and some layers are dedicated to specific tasks. Adopted from [40].

target domain, the more domain-invariant the model becomes.

C. Limitations

Current datasets and evaluation procedures are still insufficient to enable the deployment of DL-based spacecraft pose estimation algorithms in space missions. We identify key limitations below.

1) *Realism of Synthetically Generated Datasets*: One factor increasing the domain gap is the realism of the synthetic images used to train the models. The question of rendering

TABLE V: Datasets used and data augmentations applied with different pose estimation algorithms

Algorithm	Datasets Used	Data Augmentations Applied
EPFL_cvlab [35]	SPEED	Rotation, addition of random noise, zooming and cropping
SLAB Baseline [34]	SPEED, PRISMA12K, PRISMA25	Random variations in brightness and contrast, random flipping, rotation at 90 degree intervals and addition of random Gaussian noise. Also, RoI enlargement and RoI shifting are applied specifically for object detector training.
STAR LAB key-point method [25]	SPEED, URSO-OrViS	Rotation, translation, coarse dropout, addition of Gaussian noise, random brightness and contrast variations applied for training keypoint prediction network
Black et al. [29]	SPEED, Cygnus	Randomised flips, 90 degree rotations and crops applied for object detector training. Random translation and expansions, random flips, 90 degree rotations, brightness, contrast, and saturation augmentations applied for keypoint prediction training.
Wide-Depth-Range [36]	SPEED, SwissCube	Random shift, scale and rotation
LSPnet [43]	SPEED	Centre data augmentation
URSONet [41]	SPEED, URSO-OrViS	Change in image exposure and contrast, addition of Additive White Gaussian (AWG) noise, blurring and drop out of patches, random camera orientation perturbations and random plane rotations (only for SPEED dataset)
Mobile-URSONet [42]	SPEED	Random rotation of the camera across the roll axis with a maximum magnitude of 25 degrees, Gaussian blur, random changes to brightness, contrast, saturation, and hue
Huang et al. [44]	SPEED, URSO	Change in image exposure and contrast, addition of AWG noise, blurring and drop out patches, random camera orientation perturbations and random plane rotations (only for SPEED)
Lotti et al. [31]	SPEED, CPD	Random image rotations, bounding box enlargement and shifts, random brightness, and contrast adjustments
Kecen et al. [32]	SPEED	Same as SLAB Baseline
SPNv2 [40]	SPEED+	Style augmentation via neural style transfer, brightness and contrast, random erase, sun flare, blur (motion blur, median blur, glass blur), noise (Gaussian noise, ISO noise)
Sharma et al. [38]	PRISMA (Imitation-25)	Horizontal reflection, addition of zero mean white Gaussian noise
CA-SpaceNet [33]	SPEED, SwissCube	Random shift, scale, and rotation
Legrand et al. [37]	SPEED	Random variations in brightness and contrast, Gaussian noise augmentations, random rotations, and random background data augmentation

realistic images is a hard topic in the context of space because it involves simulating the behaviour of light and its interaction with various materials and surfaces in space. The lack of reference points and the absence of an atmosphere make it difficult to create realistic lighting and shading effects. To achieve a realistic depiction of space, computer graphics techniques need to be tailored specifically to the unique properties of space environments. Therefore, the question of how to render more realistic synthetic space images is a challenging and open research topic.

2) *Algorithm Evaluation*: While several attempts have been made to mitigate the domain gap between synthetic and laboratory images, there persists a one-order-of-magnitude difference between the best pose scores in the 2019 (synthetic test images) and 2021 (laboratory test images) editions of ESA’s Satellite Pose Estimation Challenge [19], [121]. Moreover, ensuring that an algorithm trained on synthetic images (source domain) performs well on laboratory images (target domain) does not guarantee that the performance level will be

maintained for space images, mainly as a result of the domain gap between the two environments.

IV. FUTURE RESEARCH DIRECTIONS

Despite the recent progress in spacecraft pose estimation, there is room for improvement in algorithm development and data generation (or collection). This section summarises open research questions and possible future directions for the field.

A. Deployability of Algorithms

The end goal of developing spacecraft pose estimation algorithms is to deploy them in space-borne hardware with limited resources. However, most existing algorithms are tested on workstations and large server clusters and very limited evaluations have been conducted on edge systems with FPGA [101], [102] or GPU [161]–[163]-based AI accelerators for space applications. In this context, this survey has made an effort to perform a trade-off comparison between the number of parameters (which can be a measure of resource consumption in the deployed hardware) in the DL models used

and the algorithm performance. However, the lack of relevant information reported makes this difficult. In future works, it would be valuable for authors to report additional metrics such as size, number of FLOPS and latency, which are suitable measures for estimating the deployability of algorithms.

Another future direction is to develop novel DL models specifically suited for edge AI accelerators. Unlike common-place Nvidia GPUs, AI accelerators for space systems support only a limited number of network layers and operations [164]. DL models with unsupported layers will have difficulty to work on such devices. Techniques like Neural Architecture Search (NAS) [165] can be used for developing efficient DL models which are deployable in space systems.

B. Explainability of Algorithms

In real-world applications, the explainability of algorithms is a key factor in determining their reliability and trustworthiness. Especially in safety-critical applications like in space, it is important to know why and how a decision / prediction was made. However, the black-box nature of DL models makes them weak for interpreting their inference processes and final results. This makes explainability difficult in DL-based spacecraft pose estimation, especially for direct end-to-end algorithms. Recently, eXplainable-AI (XAI) [166] has become a hot research topic, with new methods developed [167], [168]. Several of these proposed methods, like Bayesian deep learning [169] or conformal inference methods [170]–[172] can be applied to spacecraft pose estimation improving their explainability, which are interesting directions for future research.

C. Multi-Modal Spacecraft Pose Estimation

Most existing methods focus on visible-range images only. However, visible cameras are likely to suffer from difficult acquisition conditions in space (e.g., low light, overexposure). Therefore, other sensor such as thermal and time-of-flight of event cameras need to be considered in order to extend the operational range of classical computer vision methods. Till now, only a few works have investigated multi-modality for spacecraft pose estimation [173]–[176] which is a direction of interest for the future of vision-based navigation in space.

D. Generation of More Realistic Synthetic Data

As mentioned in section III, the main issue with the application of machine learning to space applications is the lack of data. Moreover, the ubiquitous resort to synthetic data is the source of the current domain gap problem faced in the literature. Addressing this problem could be done through a deep analysis of the rendering engines' images compared to actual space imagery. The results of this analysis could serve as the starting point for developing a rendering engine dedicated to generating realistic data for model training. To the best of our knowledge, PANGU [139] is the only initiative on this track to date. Another approach for simulation-to-real, is to introduce a physics informed layer into a deep learning system, as for example in [177]. This may induce invariance to lighting

conditions in images of satellites that result from complex lighting and shadowing conditions for satellites orbiting the Earth, such as from reflections from the satellite itself, from the Earth's surface, and from the moon's surface.

E. Domain Adaptation

One of the main obstacles to the deployment of DL-based pose estimation methods in space is the performance gap when the models are trained on synthetic images and tested on real ones. The second edition of the ESA Pose Estimation Challenge [121] was specifically designed to address this challenge, with one synthetic training and two lab test datasets. Winning methods [20] have taken advantage of dedicated learning approaches, such as self-supervised, multi-task or adversarial learning. Together with the generation of more realistic synthetic datasets for training, domain adaptation is likely to receive much interest in the coming years to overcome the domain gap problem.

F. Beyond Target-Specific Spacecraft Pose Estimation

Current algorithms estimate the pose of a single type of spacecraft at a time. For every additional spacecraft, a new dataset has to be generated and the algorithm needs to be retrained. However, with the increasing number of spacecraft launched yearly, a natural way forward is to develop more generic algorithms that are not restricted to a particular spacecraft model. Especially in applications such as debris removal, the original spacecraft structure can disintegrate into geometrical shapes not seen by the algorithm during training. Generic 6D pose estimation methods for unseen objects [178] [179] can be exploited to develop spacecraft-agnostic pose estimation algorithms.

G. Multi-Frame Spacecraft Pose Estimation

Multi-frame spacecraft pose estimation refers to determining the spacecraft pose using consecutive images, thereby leveraging temporal information. Current spacecraft pose estimation algorithms consider each image frame in isolation and the pose is estimated from information extracted from this single image frame. However, in space, pose estimation algorithms are commonly used in applications such as autonomous navigation, where a sequence of consecutive images (trajectories) is available. Hence using temporal information is key to higher pose estimation accuracy and generating temporally consistent poses. Datasets like SPARK2 [57] already provide pose estimation data as trajectories. In this direction, recently proposed ChiNet [176] have used Long Short-Term Memory (LSTM) [180] units in modelling sequences of data for estimating the spacecraft pose. However, there is a rich history of video-based 6 DoF pose estimation methods leveraging temporal information in general computer vision [181]–[183]. In future, these methods can be in-cooperated into spacecraft pose estimation, especially for applications such as spacecraft related navigation.

V. CONCLUSIONS

Monocular vision-based spacecraft pose estimation has seen considerable progress with the use of DL in recent years. However, there are still fundamental concerns that need to be addressed before these algorithms are deployed in actual space scenarios. This survey highlights these limitations, both in terms of algorithms design and datasets used for training and validation/testing. With this aim, the survey first summarised the existing algorithms according to two common approaches: hybrid modular and direct end-to-end regression approaches. Algorithms were compared in terms of performance as well as the size of the network architectures used to help understand their deployability. Then the spacecraft pose estimation datasets available for training and validating/testing these methods were discussed. The data generation methods, simulators and testbeds, and strategies used to bridge the domain gap problem were also discussed in detail. Finally, the survey provides future research directions to address these limitations and to develop spacecraft pose estimation algorithms deployable in real space missions.

VI. ADDITIONAL INFORMATION

A. Publicly available algorithm implementations

- <https://github.com/BoChenYS/satellite-pose-estimation> [23]
- https://indico.esa.int/event/319/attachments/3561/4754/pose_gerard_segmentation.pdf [35]
- <https://github.com/cvlab-epfl/wide-depth-range-pose> [36]
- <https://github.com/tpark94/speedplusbaseline> [34]
- <https://github.com/pedropro/UrsoNet> [41]
- <https://github.com/possoj/Mobile-URSONet> [42]
- <https://github.com/tpark94/spnv2> [40]
- <https://github.com/Shunli-Wang/CA-SpaceNet> [33]

B. Links to the publicly available datasets

- SHIRT: <https://taehajeffpark.com/shirt/>
- SPARK2022: <https://cvi2.uni.lu/spark2022/registration/>
- SwissCube: <https://github.com/cvlab-epfl/wide-depth-range-pose>
- SPEED+: <https://zenodo.org/record/5588480>
- SPEED: <https://zenodo.org/record/6327547>
- URSO-OrViS: <https://zenodo.org/record/3279632>

REFERENCES

- [1] H. Jones, "The recent large reduction in space launch cost." 48th International Conference on Environmental Systems, 2018.
- [2] A. Witze, "2022 was a record year for space launches," Jan 2023. [Online]. Available: <https://www.nature.com/articles/d41586-023-00048-7>
- [3] J. Kreisel, "On-orbit servicing of satellites (oos): its potential market & impact," in *proceedings of 7th ESA Workshop on Advanced Space Technologies for Robotics and Automation 'ASTRA*, 2002.
- [4] W.-J. Li, D.-Y. Cheng, X.-G. Liu, Y.-B. Wang, W.-H. Shi, Z.-X. Tang, F. Gao, F.-M. Zeng, H.-Y. Chai, W.-B. Luo *et al.*, "On-orbit service (oos) of spacecraft: A review of engineering developments," *Progress in Aerospace Sciences*, vol. 108, pp. 32–120, 2019.
- [5] M. C. Wijayatunga, R. Armellin, H. Holt, L. Pirovano, and A. A. Lidtke, "Design and guidance of a multi-active debris removal mission," *Astrodynamics*, Feb. 2023. [Online]. Available: <https://link.springer.com/10.1007/s42064-023-0159-3>
- [6] C. May, "Triggers and effects of an active debris removal market," *The Aerospace Corporation, Center for Space Policy and Strategy, Tech. Rep.*, pp. 2021–01, 2021.
- [7] J. S. Llorente, A. Agenjo, C. Carrascosa, C. de Negueruela, A. Mestreau-Garreau, A. Cropp, and A. Santovincenzo, "Proba-3: Precise formation flying demonstration mission," *Acta Astronautica*, vol. 82, no. 1, pp. 38–46, 2013.
- [8] "Prisma," <https://www.ohb-sweden.se/space-missions/prisma>, accessed: April 5, 2023.
- [9] N. T. Redd, "Bringing satellites back from the dead: Mission extension vehicles give defunct spacecraft a new lease on life - [news]," *IEEE Spectrum*, vol. 57, no. 8, pp. 6–7, 2020.
- [10] R. Biesbroek, S. Aziz, A. Wolahan, S.-f. Cipolla, M. Richard-Noca, and L. Piguat, "The clearspace-1 mission: Esa and clearspace team up to remove debris," in *Proc. 8th Eur. Conf. Sp. Debris*, 2021, pp. 1–3.
- [11] G. Marullo, L. Tanzi, P. Piazzolla, and E. Vezzetti, "6d object position estimation from 2d images: a literature review," *Multimedia Tools and Applications*, pp. 1–39, 2022.
- [12] K. Park, T. Patten, and M. Vincze, "Pix2pose: Pixel-wise coordinate regression of objects for 6d pose estimation," in *Proceedings of the IEEE/CVF International Conference on Computer Vision*, 2019, pp. 7668–7677.
- [13] R. Szeliski, *Computer vision: algorithms and applications*. Springer Nature, 2022.
- [14] D. Q. Huynh, "Metrics for 3d rotations: Comparison and analysis," *Journal of Mathematical Imaging and Vision*, vol. 35, no. 2, pp. 155–164, 2009.
- [15] J. Kelsey, J. Byrne, M. Cosgrove, S. Seereeram, and R. Mehra, "Vision-based relative pose estimation for autonomous rendezvous and docking," in *2006 IEEE Aerospace Conference*, 2006, pp. 20 pp.–.
- [16] S. D', N. Amico, M. Benn, and J. L. Jørgensen, "Pose estimation of an uncooperative spacecraft from actual space imagery," *International Journal of Space Science and Engineering*, vol. 2, no. 2, p. 171, 2014. [Online]. Available: <http://www.inderscience.com/link.php?id=60600>
- [17] L. P. Cassinis, R. Fonod, and E. Gill, "Review of the robustness and applicability of monocular pose estimation systems for relative navigation with an uncooperative spacecraft," *Progress in Aerospace Sciences*, vol. 110, p. 100548, 2019.
- [18] R. Opromolla, G. Fasano, G. Rufino, and M. Grassi, "A review of cooperative and uncooperative spacecraft pose determination techniques for close-proximity operations," *Progress in Aerospace Sciences*, vol. 93, pp. 53–72, 2017.
- [19] M. Kisantal, S. Sharma, T. H. Park, D. Izzo, M. Märtens, and S. D'Amico, "Satellite pose estimation challenge: Dataset, competition design, and results," *IEEE Transactions on Aerospace and Electronic Systems*, vol. 56, no. 5, pp. 4083–4098, 2020.
- [20] T. H. Park, M. Märtens, M. Jawaid, Z. Wang, B. Chen, T.-J. Chin, D. Izzo, and S. D'Amico, "Satellite pose estimation competition 2021: Results and analyses," *Acta Astronautica*, 2023.
- [21] J. Wang, C. Lan, C. Liu, Y. Ouyang, T. Qin, W. Lu, Y. Chen, W. Zeng, and P. Yu, "Generalizing to unseen domains: A survey on domain generalization," *IEEE Transactions on Knowledge and Data Engineering*, 2022.
- [22] J. Song, D. Rondao, and N. Aouf, "Deep learning-based spacecraft relative navigation methods: A survey," *Acta Astronautica*, vol. 191, pp. 22–40, 2022.
- [23] B. Chen, J. Cao, A. Parra, and T.-J. Chin, "Satellite pose estimation with deep landmark regression and nonlinear pose refinement," in *Proceedings of the IEEE/CVF International Conference on Computer Vision (ICCV) Workshops*, Oct 2019.
- [24] W. Huan, M. Liu, and Q. Hu, "Pose estimation for non-cooperative spacecraft based on deep learning," in *2020 39th Chinese Control Conference (CCC)*. IEEE, 2020, pp. 3339–3343.
- [25] A. Rathinam and Y. Gao, "On-orbit relative navigation near a known target using monocular vision and convolutional neural networks for pose estimation," in *International Symposium on Artificial Intelligence, Robotics and Automation in Space (iSAIRAS), Virtual Conference (Pasadena, CA:)*, 2020, pp. 1–6.
- [26] T. H. Park, S. Sharma, and S. D'Amico, "Towards robust learning-based pose estimation of noncooperative spacecraft," *arXiv preprint arXiv:1909.00392*, 2019.
- [27] Y. Huo, Z. Li, and F. Zhang, "Fast and accurate spacecraft pose estimation from single shot space imagery using box reliability and keypoints existence judgments," *IEEE Access*, vol. 8, pp. 216 283–216 297, 2020.
- [28] M. Piazza, M. Maestrini, P. Di Lizia *et al.*, "Deep learning-based monocular relative pose estimation of uncooperative spacecraft," in *8th European Conference on Space Debris, ESA/ESOC*. ESA, 2021, pp. 1–13.
- [29] K. Black, S. Shankar, D. Fonseka, J. Deutsch, A. Dhir, and M. R. Akella, "Real-time, flight-ready, non-cooperative spacecraft pose estimation using monocular imagery," *arXiv preprint arXiv:2101.09553*, 2021.
- [30] K. Cosmas and A. Kenichi, "Utilization of fpga for onboard inference of landmark localization in cnn-based spacecraft pose estimation," *Aerospace*, vol. 7, no. 11, p. 159, 2020.
- [31] A. Lotti, D. Modenini, P. Tortora, M. Saponara, and M. A. Perino, "Deep Learning for Real Time Satellite Pose Estimation on Low Power Edge TPU," *arXiv e-prints*, p. arXiv:2204.03296, Apr. 2022.
- [32] K. Li, H. Zhang, and C. Hu, "Learning-based pose estimation of non-cooperative spacecrafts with uncertainty prediction," *Aerospace*, vol. 9, no. 10, 2022. [Online]. Available: <https://www.mdpi.com/2226-4310/9/10/592>
- [33] S. Wang, S. Wang, B. Jiao, D. Yang, L. Su, P. Zhai, C. Chen, and L. Zhang, "CA-SpaceNet: Counterfactual Analysis for 6D Pose Estimation in Space," *arXiv e-prints*, p. arXiv:2207.07869, Jul. 2022.
- [34] T. H. Park, S. Sharma, and S. D'Amico, "Towards robust learning-based pose estimation of noncooperative spacecraft," *arXiv preprint arXiv:1909.00392*, 2019.
- [35] K. Gerard, "Segmentation-driven satellite pose estimation," Technical Report. EPFL. Available online at: <https://indico.esa.int/event...>, Tech. Rep., 2019.
- [36] Y. Hu, S. Speierer, W. Jakob, P. Fua, and M. Salzmann, "Wide-depth-range 6d object pose estimation in space," in *Proceedings of the IEEE/CVF Conference on Computer Vision and Pattern Recognition*, 2021, pp. 15 870–15 879.
- [37] A. Legrand, R. Detry, and C. De Vleeschouwer, "End-to-end neural estimation of spacecraft pose with intermediate detection of keypoints." S. Sharma, C. Beierle, and S. D'Amico, "Pose estimation for non-cooperative spacecraft rendezvous using convolutional neural networks," in *2018 IEEE Aerospace Conference*. IEEE, 2018, pp. 1–12.
- [38] S. Sharma and S. D'Amico, "Pose estimation for non-cooperative rendezvous using neural networks," *arXiv preprint arXiv:1906.09868*, 2019.
- [39] T. H. Park and S. D'Amico, "Robust multi-task learning and online refinement for spacecraft pose estimation across domain gap," *arXiv preprint arXiv:2203.04275*, 2022.
- [40] P. F. Proença and Y. Gao, "Deep learning for spacecraft pose estimation from photorealistic rendering," in *2020 IEEE International Conference on Robotics and Automation (ICRA)*. IEEE, 2020, pp. 6007–6013.
- [41] J. Posso, G. Bois, and Y. Savaria, "Mobile-ursonet: an embeddable neural network for onboard spacecraft pose estimation," *arXiv preprint arXiv:2205.02065*, 2022.
- [42] A. Garcia, M. A. Musallam, V. Gaudilliere, E. Ghorbel, K. Al Ismaeil, M. Perez, and D. Aouada, "Lspnet: A 2d localization-oriented spacecraft pose estimation neural network," in *Proceedings of the IEEE/CVF Conference on Computer Vision and Pattern Recognition*, 2021, pp. 2048–2056.
- [43] H. Huang, G. Zhao, D. Gu, and Y. Bo, "Non-model-based monocular pose estimation network for uncooperative spacecraft using convolu-

- tional neural network,” *IEEE Sensors Journal*, vol. 21, no. 21, pp. 24 579–24 590, 2021.
- [45] T. Phisannupawong, P. Kamsing, P. Torteeka, S. Channumsin, U. Sawangwit, W. Hematulin, T. Jarawan, T. Somjit, S. Yooyen, D. Delahaye *et al.*, “Vision-based spacecraft pose estimation via a deep convolutional neural network for noncooperative docking operations,” *Aerospace*, vol. 7, no. 9, p. 126, 2020.
 - [46] A. Voulodimos, N. Doulamis, A. Doulamis, and E. Protopapadakis, “Deep learning for computer vision: A brief review,” *Computational intelligence and neuroscience*, vol. 2018, 2018.
 - [47] J. Chai, H. Zeng, A. Li, and E. W. Ngai, “Deep learning in computer vision: A critical review of emerging techniques and application scenarios,” *Machine Learning with Applications*, vol. 6, p. 100134, 2021.
 - [48] W. Wang, Y. Yang, X. Wang, W. Wang, and J. Li, “Development of convolutional neural network and its application in image classification: a survey,” *Optical Engineering*, vol. 58, no. 4, pp. 040 901–040 901, 2019.
 - [49] S. Minaee, Y. Y. Boykov, F. Porikli, A. J. Plaza, N. Kehtarnavaz, and D. Terzopoulos, “Image segmentation using deep learning: A survey,” *IEEE transactions on pattern analysis and machine intelligence*, 2021.
 - [50] G. Ciaparrone, F. L. Sánchez, S. Tabik, L. Troiano, R. Tagliaferri, and F. Herrera, “Deep learning in video multi-object tracking: A survey,” *Neurocomputing*, vol. 381, pp. 61–88, 2020.
 - [51] S. D’Amico, M. Benn, and J. L. Jørgensen, “Pose estimation of an uncooperative spacecraft from actual space imagery,” *International Journal of Space Science and Engineering* 5, vol. 2, no. 2, pp. 171–189, 2014.
 - [52] J. Shi, S. Ulrich, and S. Ruel, “Spacecraft pose estimation using a monocular camera,” in *67th International Astronautical Congress*. Guadalajara, 2016.
 - [53] C. Liu and W. Hu, “Relative pose estimation for cylinder-shaped spacecrafts using single image,” *IEEE Transactions on Aerospace and Electronic Systems*, vol. 50, no. 4, pp. 3036–3056, 2014.
 - [54] S. Sharma, J. Ventura, and S. D’Amico, “Robust model-based monocular pose initialization for noncooperative spacecraft rendezvous,” *Journal of Spacecraft and Rockets*, vol. 55, no. 6, pp. 1414–1429, 2018.
 - [55] D. Rondao and N. Aouf, “Multi-view monocular pose estimation for spacecraft relative navigation,” in *2018 AIAA Guidance, Navigation, and Control Conference*, 2018, p. 2100.
 - [56] V. Capuano, S. R. Alimo, A. Q. Ho, and S.-J. Chung, “Robust features extraction for on-board monocular-based spacecraft pose acquisition,” in *AIAA Scitech 2019 Forum*, 2019, p. 2005.
 - [57] A. Rathinam, V. Gaudilliere, M. A. Mohamed Ali, M. Ortiz Del Castillo, L. Pauly, and D. Aouada, “SPARK 2022 Dataset : Spacecraft Detection and Trajectory Estimation,” Jun. 2022. [Online]. Available: <https://doi.org/10.5281/zenodo.6599762>
 - [58] L. Jiao, F. Zhang, F. Liu, S. Yang, L. Li, Z. Feng, and R. Qu, “A survey of deep learning-based object detection,” *IEEE access*, vol. 7, pp. 128 837–128 868, 2019.
 - [59] S. Ren, K. He, R. Girshick, and J. Sun, “Faster r-cnn: Towards real-time object detection with region proposal networks,” *Advances in neural information processing systems*, vol. 28, 2015.
 - [60] K. He, G. Gkioxari, P. Dollár, and R. Girshick, “Mask r-cnn,” in *Proceedings of the IEEE international conference on computer vision*, 2017, pp. 2961–2969.
 - [61] J. Redmon, S. Divvala, R. Girshick, and A. Farhadi, “You only look once: Unified, real-time object detection,” in *Proceedings of the IEEE conference on computer vision and pattern recognition*, 2016, pp. 779–788.
 - [62] W. Liu, D. Anguelov, D. Erhan, C. Szegedy, S. Reed, C.-Y. Fu, and A. C. Berg, “Ssd: Single shot multibox detector,” in *European conference on computer vision*. Springer, 2016, pp. 21–37.
 - [63] Y. Xiong, H. Liu, S. Gupta, B. Akin, G. Bender, Y. Wang, P.-J. Kindermans, M. Tan, V. Singh, and B. Chen, “Mobilenets: Searching for object detection architectures for mobile accelerators,” in *Proceedings of the IEEE/CVF Conference on Computer Vision and Pattern Recognition*, 2021, pp. 3825–3834.
 - [64] S. S. A. Zaidi, M. S. Ansari, A. Aslam, N. Kanwal, M. Asghar, and B. Lee, “A survey of modern deep learning based object detection models,” *Digital Signal Processing*, p. 103514, 2022.
 - [65] Z. Zou, Z. Shi, Y. Guo, and J. Ye, “Object detection in 20 years: A survey,” *arXiv preprint arXiv:1905.05055*, 2019.
 - [66] B. Chen, J. Cao, A. Parra, and T.-J. Chin, “Satellite pose estimation with deep landmark regression and nonlinear pose refinement,” in *Proceedings of the IEEE/CVF International Conference on Computer Vision Workshops*, 2019, pp. 0–0.
 - [67] A. Price and K. Yoshida, “A monocular pose estimation case study: The hayabusa2 minerva-ii2 deployment,” in *Proceedings of the IEEE/CVF Conference on Computer Vision and Pattern Recognition*, 2021, pp. 1992–2001.
 - [68] R. Hartley and A. Zisserman, *Multiple view geometry in computer vision*. Cambridge university press, 2003.
 - [69] J. Wang, K. Sun, T. Cheng, B. Jiang, C. Deng, Y. Zhao, D. Liu, Y. Mu, M. Tan, X. Wang *et al.*, “Deep high-resolution representation learning for visual recognition,” *IEEE transactions on pattern analysis and machine intelligence*, vol. 43, no. 10, pp. 3349–3364, 2020.
 - [70] J. Redmon and A. Farhadi, “Yolo9000: better, faster, stronger,” in *Proceedings of the IEEE conference on computer vision and pattern recognition*, 2017, pp. 7263–7271.
 - [71] M. Sandler, A. Howard, M. Zhu, A. Zhmoginov, and L.-C. Chen, “Mobilenetv2: Inverted residuals and linear bottlenecks,” in *Proceedings of the IEEE conference on computer vision and pattern recognition*, 2018, pp. 4510–4520.
 - [72] Tensorflow, “Tpu/models/official/efficientnet/lite at master · tensorflow/tpu.” [Online]. Available: <https://github.com/tensorflow/tpu/tree/master/models/official/efficientnet/lite>
 - [73] M. Tan and Q. Le, “Efficientnet: Rethinking model scaling for convolutional neural networks,” in *International conference on machine learning*. PMLR, 2019, pp. 6105–6114.
 - [74] Y. Hu, J. Hugonot, P. Fua, and M. Salzmann, “Segmentation-driven 6d object pose estimation,” in *Proceedings of the IEEE/CVF Conference on Computer Vision and Pattern Recognition*, 2019, pp. 3385–3394.
 - [75] A. Howard, M. Sandler, G. Chu, L.-C. Chen, B. Chen, M. Tan, W. Wang, Y. Zhu, R. Pang, V. Vasudevan *et al.*, “Searching for mobilenetv3,” in *Proceedings of the IEEE/CVF international conference on computer vision*, 2019, pp. 1314–1324.
 - [76] B. Cheng, B. Xiao, J. Wang, H. Shi, T. S. Huang, and L. Zhang, “High-erhmet: Scale-aware representation learning for bottom-up human pose estimation,” in *Proceedings of the IEEE/CVF Conference on Computer Vision and Pattern Recognition*, 2020, pp. 5386–5395.
 - [77] O. Ronneberger, P. Fischer, and T. Brox, “U-net: Convolutional networks for biomedical image segmentation,” in *International Conference on Medical image computing and computer-assisted intervention*. Springer, 2015, pp. 234–241.
 - [78] A. Bochkovskiy, C.-Y. Wang, and H.-Y. M. Liao, “Yolov4: Optimal speed and accuracy of object detection,” *arXiv preprint arXiv:2004.10934*, 2020.
 - [79] T.-Y. Lin, P. Dollár, R. Girshick, K. He, B. Hariharan, and S. Belongie, “Feature pyramid networks for object detection,” in *Proceedings of the IEEE conference on computer vision and pattern recognition*, 2017, pp. 2117–2125.
 - [80] J. Pearl and D. Mackenzie, *The book of why: the new science of cause and effect*. Basic books, 2018.
 - [81] E. Marchand, H. Uchiyama, and F. Spindler, “Pose estimation for augmented reality: a hands-on survey,” *IEEE transactions on visualization and computer graphics*, vol. 22, no. 12, pp. 2633–2651, 2015.
 - [82] M. A. Fischler and R. C. Bolles, “Random sample consensus: a paradigm for model fitting with applications to image analysis and automated cartography,” *Communications of the ACM*, vol. 24, no. 6, pp. 381–395, 1981.
 - [83] T. Strutz, *Data fitting and uncertainty: A practical introduction to weighted least squares and beyond*. Springer, 2011.
 - [84] “Perspective-n-point (pnp) pose computation.” [Online]. Available: https://docs.opencv.org/4.x/d5/d1f/calib3d_solvePnP.html
 - [85] V. Lepetit, F. Moreno-Noguer, and P. Fua, “Eppnp: An accurate o (n) solution to the pnp problem,” *International journal of computer vision*, vol. 81, no. 2, p. 155, 2009.
 - [86] Y. Hu, P. Fua, W. Wang, and M. Salzmann, “Single-stage 6d object pose estimation,” in *Proceedings of the IEEE/CVF conference on computer vision and pattern recognition*, 2020, pp. 2930–2939.
 - [87] A. Kendall and R. Cipolla, “Geometric loss functions for camera pose regression with deep learning,” in *Proceedings of the IEEE conference on computer vision and pattern recognition*, 2017, pp. 5974–5983.
 - [88] C. Szegedy, W. Liu, Y. Jia, P. Sermanet, S. Reed, D. Anguelov, D. Erhan, V. Vanhoucke, and A. Rabinovich, “Going deeper with

- convolutions,” in *Proceedings of the IEEE conference on computer vision and pattern recognition*, 2015, pp. 1–9.
- [89] A. Krizhevsky, I. Sutskever, and G. E. Hinton, “Imagenet classification with deep convolutional neural networks,” *Communications of the ACM*, vol. 60, pp. 84–90, 2012.
- [90] Q. Wang, Y. Ma, K. Zhao, and Y. Tian, “A comprehensive survey of loss functions in machine learning,” *Annals of Data Science*, vol. 9, no. 2, pp. 187–212, 2022.
- [91] R. C. Mittelhammer, G. G. Judge, and D. J. Miller, *Econometric foundations*. Cambridge University Press, 2000.
- [92] K. He, X. Zhang, S. Ren, and J. Sun, “Deep residual learning for image recognition,” in *Proceedings of the IEEE conference on computer vision and pattern recognition*, 2016, pp. 770–778.
- [93] J. Hu, L. Shen, and G. Sun, “Squeeze-and-excitation networks,” in *Proceedings of the IEEE conference on computer vision and pattern recognition*, 2018, pp. 7132–7141.
- [94] Y. Bukschat and M. Vetter, “Efficientpose: An efficient, accurate and scalable end-to-end 6d multi object pose estimation approach,” *arXiv preprint arXiv:2011.04307*, 2020.
- [95] M. Tan, R. Pang, and Q. V. Le, “Efficientdet: Scalable and efficient object detection,” in *Proceedings of the IEEE/CVF conference on computer vision and pattern recognition*, 2020, pp. 10 781–10 790.
- [96] C. E. Shannon, “A mathematical theory of communication,” *The Bell system technical journal*, vol. 27, no. 3, pp. 379–423, 1948.
- [97] A. Lotti, D. Modenini, P. Tortora, M. Saponara, and M. A. Perino, “Deep learning for real time satellite pose estimation on low power edge tpu,” *arXiv preprint arXiv:2204.03296*, 2022.
- [98] R. Hadidi, J. Cao, Y. Xie, B. Asgari, T. Krishna, and H. Kim, “Characterizing the deployment of deep neural networks on commercial edge devices,” in *2019 IEEE International Symposium on Workload Characterization (IISWC)*. IEEE, 2019, pp. 35–48.
- [99] S. P. Baller, A. Jindal, M. Chadha, and M. Gerndt, “Deepedgebench: Benchmarking deep neural networks on edge devices,” in *2021 IEEE International Conference on Cloud Engineering (IC2E)*. IEEE, 2021, pp. 20–30.
- [100] Xilinx. (2022) Product guide: Dpucdzx8g for zynq ultrascale+ mpsocs. [Online]. Available: https://www.xilinx.com/content/dam/xilinx/support/documents/ip_documentation/dpu/v4_0/pg338-dpu.pdf
- [101] G. Furano, G. Meoni, A. Dunne, D. Moloney, V. Ferlet-Cavrois, A. Tavoularis, J. Byrne, L. Buckley, M. Psarakis, K.-O. Voss *et al.*, “Towards the use of artificial intelligence on the edge in space systems: Challenges and opportunities,” *IEEE Aerospace and Electronic Systems Magazine*, vol. 35, no. 12, pp. 44–56, 2020.
- [102] V. Leon, G. Lentaris, D. Soudris, S. Vellas, and M. Bernou, “Towards employing fpga and asip acceleration to enable onboard ai/ml in space applications,” in *2022 IFIP/IEEE 30th International Conference on Very Large Scale Integration (VLSI-SoC)*. IEEE, 2022, pp. 1–4.
- [103] C. B. Azodi, J. Tang, and S.-H. Shiu, “Opening the black box: interpretable machine learning for geneticists,” *Trends in genetics*, vol. 36, no. 6, pp. 442–455, 2020.
- [104] O. Li, H. Liu, C. Chen, and C. Rudin, “Deep learning for case-based reasoning through prototypes: A neural network that explains its predictions,” in *Proceedings of the AAAI Conference on Artificial Intelligence*, vol. 32, no. 1, 2018.
- [105] H. Wang and D.-Y. Yeung, “A survey on bayesian deep learning,” *ACM computing surveys (csur)*, vol. 53, no. 5, pp. 1–37, 2020.
- [106] K. Sun, Y. Zhao, B. Jiang, T. Cheng, B. Xiao, D. Liu, Y. Mu, X. Wang, W. Liu, and J. Wang, “High-resolution representations for labeling pixels and regions,” *arXiv preprint arXiv:1904.04514*, 2019.
- [107] K. Sun, B. Xiao, D. Liu, and J. Wang, “Deep high-resolution representation learning for human pose estimation,” in *Proceedings of the IEEE/CVF conference on computer vision and pattern recognition*, 2019, pp. 5693–5703.
- [108] J. Redmon and A. Farhadi, “Yolov3: An incremental improvement,” *arXiv preprint arXiv:1804.02767*, 2018.
- [109] X. Long, K. Deng, G. Wang, Y. Zhang, Q. Dang, Y. Gao, H. Shen, J. Ren, S. Han, E. Ding *et al.*, “Pp-yolo: An effective and efficient implementation of object detector,” *arXiv preprint arXiv:2007.12099*, 2020.
- [110] J. J. Moré, “The levenberg-marquardt algorithm: implementation and theory,” in *Numerical analysis*. Springer, 1978, pp. 105–116.
- [111] Z. Cai and N. Vasconcelos, “Cascade r-cnn: Delving into high quality object detection,” in *Proceedings of the IEEE conference on computer vision and pattern recognition*, 2018, pp. 6154–6162.
- [112] M. C. Leong, D. K. Prasad, Y. T. Lee, and F. Lin, “Semi-cnn architecture for effective spatio-temporal learning in action recognition,” *Applied Sciences*, vol. 10, no. 2, p. 557, 2020.
- [113] T. Hou, A. Ahmadyan, L. Zhang, J. Wei, and M. Grundmann, “Mobile-pose: Real-time pose estimation for unseen objects with weak shape supervision,” *arXiv preprint arXiv:2003.03522*, 2020.
- [114] X. Long, K. Deng, G. Wang, Y. Zhang, Q. Dang, Y. Gao, H. Shen, J. Ren, S. Han, E. Ding *et al.*, “Pp-yolo: An effective and efficient implementation of object detector,” *arXiv preprint arXiv:2007.12099*, 2020.
- [115] M. C. Leong, D. K. Prasad, Y. T. Lee, and F. Lin, “Semi-cnn architecture for effective spatio-temporal learning in action recognition,” *Applied Sciences*, vol. 10, no. 2, p. 557, 2020.
- [116] Z. Ge, S. Liu, F. Wang, Z. Li, and J. Sun, “Yolox: Exceeding yolo series in 2021,” *arXiv preprint arXiv:2107.08430*, 2021.
- [117] S. Hinterstoisser, V. Lepetit, S. Ilic, S. Holzer, G. R. Bradski, K. Konolige, and N. Navab, “Model based training, detection and pose estimation of texture-less 3d objects in heavily cluttered scenes,” in *Asian Conference on Computer Vision*, 2012.
- [118] J. Deng, W. Dong, R. Socher, L.-J. Li, K. Li, and L. Fei-Fei, “Imagenet: A large-scale hierarchical image database,” in *2009 IEEE conference on computer vision and pattern recognition*. Ieee, 2009, pp. 248–255.
- [119] A. Kendall, M. Grimes, and R. Cipolla, “PoseNet: A Convolutional Network for Real-Time 6-DOF Camera Relocalization,” *arXiv e-prints*, p. arXiv:1505.07427, May 2015.
- [120] T. H. Park and S. D’Amico, “Adaptive neural network-based unscented kalman filter for spacecraft pose tracking at rendezvous,” *arXiv preprint arXiv:2206.03796*, 2022.
- [121] T. H. Park, M. Märtens, M. Jawaid, Z. Wang, B. Chen, T.-J. Chin, D. Izzo, and S. D’Amico, “Satellite pose estimation competition 2021: Results and analyses,” *Acta Astronautica*, vol. 204, pp. 640–665, 2023. [Online]. Available: <https://www.sciencedirect.com/science/article/pii/S0094576523000048>
- [122] T. Lin, M. Maire, S. J. Belongie, J. Hays, P. Perona, D. Ramanan, P. Dollár, and C. L. Zitnick, “Microsoft COCO: common objects in context,” in *Computer Vision - ECCV 2014 - 13th European Conference, Zurich, Switzerland, September 6-12, 2014, Proceedings, Part V*, ser. Lecture Notes in Computer Science, D. J. Fleet, T. Pajdla, B. Schiele, and T. Tuytelaars, Eds., vol. 8693. Springer, 2014, pp. 740–755. [Online]. Available: https://doi.org/10.1007/978-3-319-10602-1_48
- [123] O. Russakovsky, J. Deng, H. Su, J. Krause, S. Satheesh, S. Ma, Z. Huang, A. Karpathy, A. Khosla, M. S. Bernstein, A. C. Berg, and L. Fei-Fei, “Imagenet large scale visual recognition challenge,” *Int. J. Comput. Vis.*, vol. 115, no. 3, pp. 211–252, 2015. [Online]. Available: <https://doi.org/10.1007/s11263-015-0816-y>
- [124] Y. Song, T. Wang, S. K. Mondal, and J. P. Sahoo, “A comprehensive survey of few-shot learning: Evolution, applications, challenges, and opportunities,” *arXiv preprint arXiv:2205.06743*, 2022.
- [125] W. Cao, C. Zhou, Y. Wu, Z. Ming, Z. Xu, and J. Zhang, “Research progress of zero-shot learning beyond computer vision,” in *Algorithms and Architectures for Parallel Processing: 20th International Conference, ICA3PP 2020, New York City, NY, USA, October 2–4, 2020, Proceedings, Part II 20*. Springer, 2020, pp. 538–551.
- [126] C. Rennie, R. Shome, K. E. Bekris, and A. F. D. Souza, “A dataset for improved rgbd-based object detection and pose estimation for warehouse pick-and-place,” *IEEE Robotics Autom. Lett.*, vol. 1, no. 2, pp. 1179–1185, 2016. [Online]. Available: <https://doi.org/10.1109/LRA.2016.2532924>
- [127] Y. Xiang, T. Schmidt, V. Narayanan, and D. Fox, “Posecnn: A convolutional neural network for 6d object pose estimation in cluttered scenes,” in *Robotics: Science and Systems XIV, Carnegie Mellon University, Pittsburgh, Pennsylvania, USA, June 26-30, 2018*, H. Kress-Gazit, S. S. Srinivasa, T. Howard, and N. Atanasov, Eds., 2018. [Online]. Available: <http://www.roboticsproceedings.org/rss14/p19.html>
- [128] L. Pauly, M. L. Jamrozik, M. O. Del Castillo, O. Borgue, I. P. Singh, M. R. Makhdoom, O.-O. Christidi-Loumpasfiski, V. Gaudilliere, C. Martinez, A. Rathinam *et al.*, “Lessons from a space lab—an image acquisition perspective,” *arXiv preprint arXiv:2208.08865*, 2022.
- [129] T. H. Park, J. Bosse, and S. D’Amico, “Robotic testbed for rendezvous and optical navigation: Multi-source calibration and machine learning use cases,” *arXiv preprint arXiv:2108.05529*, 2021.

- [130] M. Sabatini, G. B. Palmerini, and P. Gasbarri, "A testbed for visual based navigation and control during space rendezvous operations," *Acta Astronautica*, vol. 117, pp. 184–196, 2015. [Online]. Available: <https://www.sciencedirect.com/science/article/pii/S0094576515003070>
- [131] Y. Fang, P.-T. Yap, W. Lin, H. Zhu, and M. Liu, "Source-free unsupervised domain adaptation: A survey," *arXiv preprint arXiv:2301.00265*, 2022.
- [132] M. Wang and W. Deng, "Deep visual domain adaptation: A survey," *Neurocomputing*, vol. 312, pp. 135–153, 2018.
- [133] T.-Y. Lin, M. Maire, S. Belongie, J. Hays, P. Perona, D. Ramanan, P. Dollár, and C. L. Zitnick, "Microsoft coco: Common objects in context," in *Computer Vision—ECCV 2014: 13th European Conference, Zurich, Switzerland, September 6–12, 2014, Proceedings, Part V 13*. Springer, 2014, pp. 740–755.
- [134] E. S. A. (ESA), "Prisma's tango and mango satellites," https://www.esa.int/ESA_Multimedia/Images/2010/10/Prisma_s_Tango_and_Mango_satellites, 2010, accessed: 05-April-2023.
- [135] V. Gaudillière, L. Pauly, A. Rathinam, A. G. Sanchez, M. A. Musallam, and D. Aouada, "3d-aware object localization using gaussian implicit occupancy function," *arXiv preprint arXiv:2303.02058*, 2023.
- [136] A. Mertan, D. J. Duff, and G. Unal, "Single image depth estimation: An overview," *Digital Signal Processing*, p. 103441, 2022.
- [137] S. Yuheng and Y. Hao, "Image segmentation algorithms overview," *arXiv preprint arXiv:1707.02051*, 2017.
- [138] Y. Wang, X. Shen, S. X. Hu, Y. Yuan, J. L. Crowley, and D. Vaufraydaz, "Self-supervised transformers for unsupervised object discovery using normalized cut," in *Proceedings of the IEEE/CVF Conference on Computer Vision and Pattern Recognition*, 2022, pp. 14 543–14 553.
- [139] I. Martin, M. Dunstan, and M. S. Gestido, "Planetary surface image generation for testing future space missions with pangui," in *2nd RPI Space Imaging Workshop*. Sensing, Estimation, and Automation Laboratory, 2019.
- [140] R. Brochard, J. Lebreton, C. Robin, K. Kanani, G. Jonniaux, A. Masson, N. Despré, and A. Berjaoui, "Scientific image rendering for space scenes with the surrender software," *arXiv preprint arXiv:1810.01423*, 2018.
- [141] D. Shreiner, B. T. K. O. A. W. Group *et al.*, *OpenGL programming guide: the official guide to learning OpenGL, versions 3.0 and 3.1*. Pearson Education, 2009.
- [142] A. Rathinam, Z. Hao, and Y. Gao, "Autonomous visual navigation for spacecraft on-orbit operations," in *Space Robotics and Autonomous Systems: Technologies, advances and applications*. Institution of Engineering and Technology, Aug. 2021, pp. 125–157. [Online]. Available: https://doi.org/10.1049/PBCE131E_ch5
- [143] M. Bechini, P. Lunghi, M. Lavagna *et al.*, "Spacecraft pose estimation via monocular image processing: Dataset generation and validation," in *9th European Conference for Aerospace Sciences (EUCASS 2022)*, 2022, pp. 1–15.
- [144] C. Beierle and S. D'Amico, "Variable-magnification optical stimulator for training and validation of spaceborne vision-based navigation," *Journal of Spacecraft and Rockets*, vol. 56, no. 4, pp. 1060–1072, 2019.
- [145] P. Colmenarejo, M. Graziano, G. Novelli, D. Mora, P. Serra, A. Tomassini, K. Seweryn, G. Prisco, and J. G. Fernandez, "On ground validation of debris removal technologies," *Acta Astronautica*, vol. 158, pp. 206–219, 2019. [Online]. Available: <https://www.sciencedirect.com/science/article/pii/S0094576517312845>
- [146] GMV, "platform-art," <https://satsearch.co/services/gmv-platform-art-for-satellite-orbit-simulation>, 2018.
- [147] H. Benninghoff, F. Rems, E.-A. Risse, and C. Mietner, "European proximity operations simulator 2.0 (epos) - a robotic-based rendezvous and docking simulator," *Journal of large-scale research facilities JLSRF*, vol. 3, p. 107, 2017.
- [148] L. P. Cassinis, A. Menicucci, E. Gill, I. Ahrens, and J. G. Fernandez, "On-ground validation of a cnn-based monocular pose estimation system for uncooperative spacecraft," in *8th European Conference on Space Debris*, vol. 8, 2021.
- [149] M. Quigley, K. Conley, B. Gerkey, J. Faust, T. Foote, J. Leibs, R. Wheeler, A. Y. Ng *et al.*, "Ros: an open-source robot operating system," in *ICRA workshop on open source software*, vol. 3, no. 3.2. Kobe, Japan, 2009, p. 5.
- [150] S. Ben-David, J. Blitzer, K. Crammer, and F. Pereira, "Analysis of representations for domain adaptation," *Advances in neural information processing systems*, vol. 19, 2006.
- [151] C. Toft, W. Maddern, A. Torii, L. Hammarstrand, E. Stenborg, D. Safari, M. Okutomi, M. Pollefeys, J. Sivic, T. Pajdla *et al.*, "Long-term visual localization revisited," *IEEE Transactions on Pattern Analysis and Machine Intelligence*, 2020.
- [152] T. H. Park and S. D'Amico, "Robust multi-task learning and online refinement for spacecraft pose estimation across domain gap," *Advances in Space Research*, 2023. [Online]. Available: <https://www.sciencedirect.com/science/article/pii/S0273117723002284>
- [153] A. Mumuni and F. Mumuni, "Data augmentation: A comprehensive survey of modern approaches," *Array*, vol. 16, p. 100258, 2022. [Online]. Available: <https://www.sciencedirect.com/science/article/pii/S2590005622000911>
- [154] X. Peng, Z. Tang, F. Yang, R. S. Feris, and D. Metaxas, "Jointly optimize data augmentation and network training: Adversarial data augmentation in human pose estimation," in *Proceedings of the IEEE conference on computer vision and pattern recognition*, 2018, pp. 2226–2234.
- [155] J. Tobin, R. Fong, A. Ray, J. Schneider, W. Zaremba, and P. Abbeel, "Domain randomization for transferring deep neural networks from simulation to the real world," *2017 IEEE/RSJ International Conference on Intelligent Robots and Systems (IROS)*, pp. 23–30, 2017.
- [156] —, "Domain randomization for transferring deep neural networks from simulation to the real world," in *2017 IEEE/RSJ international conference on intelligent robots and systems (IROS)*. IEEE, 2017, pp. 23–30.
- [157] P. T. G. Jackson, A. A. Abarghouei, S. Bonner, T. P. Breckon, and B. Obara, "Style augmentation: Data augmentation via style randomization," *CoRR*, vol. abs/1809.05375, 2018. [Online]. Available: <http://arxiv.org/abs/1809.05375>
- [158] S. Ruder, "An overview of multi-task learning in deep neural networks," *arXiv preprint arXiv:1706.05098*, 2017.
- [159] C. Shui, M. Abbasi, L.-É. Robitaille, B. Wang, and C. Gagné, "A principled approach for learning task similarity in multitask learning," *arXiv preprint arXiv:1903.09109*, 2019.
- [160] Y. Ganin, E. Ustinova, H. Ajakan, P. Germain, H. Larochelle, F. Laviolette, M. Marchand, and V. Lempitsky, "Domain-adversarial training of neural networks," *The journal of machine learning research*, vol. 17, no. 1, pp. 2096–2030, 2016.
- [161] L. Kosmidis, I. Rodriguez, Á. Jover, S. Alcaide, J. Lachaize, J. Abella, O. Notebaert, F. J. Cazorla, and D. Steenari, "Gpu4s: Embedded gpus in space-latest project updates," *Microprocessors and Microsystems*, vol. 77, p. 103143, 2020.
- [162] W. Powell, M. Campola, T. Sheets, A. Davidson, and S. Welsh, "Commercial off-the-shelf gpu qualification for space applications," Tech. Rep., 2018.
- [163] F. C. Bruhn, N. Tsog, F. Kunkel, O. Flordal, and I. Troxel, "Enabling radiation tolerant heterogeneous gpu-based onboard data processing in space," *CEAS Space Journal*, vol. 12, no. 4, pp. 551–564, 2020.
- [164] A. Xilinx, "Vitis ai user guide," https://www.xilinx.com/content/dam/xilinx/support/documents/sw_manuals/vitis_ai/2_5/ug1414-vitis-ai.pdf, 15 Jun 2022, [Online; accessed 30-Jan-2023].
- [165] M. Wistuba, A. Rawat, and T. Pedapati, "A survey on neural architecture search," *arXiv preprint arXiv:1905.01392*, 2019.
- [166] D. Gunning, M. Stefik, J. Choi, T. Miller, S. Stumpf, and G.-Z. Yang, "Xai—explainable artificial intelligence," *Science robotics*, vol. 4, no. 37, p. eaay7120, 2019.
- [167] X. Bai, X. Wang, X. Liu, Q. Liu, J. Song, N. Sebe, and B. Kim, "Explainable deep learning for efficient and robust pattern recognition: A survey of recent developments," *Pattern Recognition*, vol. 120, p. 108102, 2021.
- [168] F. Xu, H. Uszkoreit, Y. Du, W. Fan, D. Zhao, and J. Zhu, "Explainable ai: A brief survey on history, research areas, approaches and challenges," in *Natural Language Processing and Chinese Computing: 8th CCF International Conference, NLPCC 2019, Dunhuang, China, October 9–14, 2019, Proceedings, Part II 8*. Springer, 2019, pp. 563–574.
- [169] A. Kendall and Y. Gal, "What uncertainties do we need in bayesian deep learning for computer vision?" *Advances in neural information processing systems*, vol. 30, 2017.
- [170] G. Shafer and V. Vovk, "A tutorial on conformal prediction," *Journal of Machine Learning Research*, vol. 9, no. 3, 2008.
- [171] A. N. Angelopoulos and S. Bates, "A gentle introduction to conformal prediction and distribution-free uncertainty quantification," *arXiv preprint arXiv:2107.07511*, 2021.

- [172] R. J. Tibshirani, R. Foygel Barber, E. Candes, and A. Ramdas, "Conformal prediction under covariate shift," in *Advances in Neural Information Processing Systems*, H. Wallach, H. Larochelle, A. Beygelzimer, F. d'Alché-Buc, E. Fox, and R. Garnett, Eds., vol. 32. Curran Associates, Inc., 2019. [Online]. Available: <https://proceedings.neurips.cc/paper/2019/file/8fb21ee7a2207526da55a679f0332de2-Paper.pdf>
- [173] M. Jawaid, E. Elms, Y. Latif, and T.-J. Chin, "Towards bridging the space domain gap for satellite pose estimation using event sensing," 2022. [Online]. Available: <https://arxiv.org/abs/2209.11945>
- [174] D. Rondao, N. Aouf, and M. A. Richardson, "Chinet: Deep recurrent convolutional learning for multimodal spacecraft pose estimation," *CoRR*, vol. abs/2108.10282, 2021. [Online]. Available: <https://arxiv.org/abs/2108.10282>
- [175] M. Hogan, D. Rondao, N. Aouf, and O. Dubois-Matra, "Using convolutional neural networks for relative pose estimation of a non-cooperative spacecraft with thermal infrared imagery," *CoRR*, vol. abs/2105.13789, 2021. [Online]. Available: <https://arxiv.org/abs/2105.13789>
- [176] D. Rondao, N. Aouf, and M. A. Richardson, "Chinet: Deep recurrent convolutional learning for multimodal spacecraft pose estimation," *IEEE Transactions on Aerospace and Electronic Systems*, 2022.
- [177] A. Lengyel, S. Garg, M. Milford, and J. C. van Gemert, "Zero-shot day-night domain adaptation with a physics prior," in *Proceedings of the IEEE/CVF International Conference on Computer Vision*, 2021, pp. 4399–4409.
- [178] M. Gou, H. Pan, H.-S. Fang, Z. Liu, C. Lu, and P. Tan, "Unseen object 6d pose estimation: a benchmark and baselines," *arXiv preprint arXiv:2206.11808*, 2022.
- [179] K. Park, A. Mousavian, Y. Xiang, and D. Fox, "Latentfusion: End-to-end differentiable reconstruction and rendering for unseen object pose estimation," in *Proceedings of the IEEE/CVF conference on computer vision and pattern recognition*, 2020, pp. 10 710–10 719.
- [180] S. Hochreiter and J. Schmidhuber, "Long short-term memory," *Neural Comput.*, vol. 9, no. 8, p. 1735–1780, nov 1997. [Online]. Available: <https://doi.org/10.1162/neco.1997.9.8.1735>
- [181] A. Beedu, Z. Ren, V. Agrawal, and I. Essa, "Videopose: Estimating 6d object pose from videos," *arXiv preprint arXiv:2111.10677*, 2021.
- [182] A. Beedu, H. Alamri, and I. Essa, "Video based object 6d pose estimation using transformers," *arXiv preprint arXiv:2210.13540*, 2022.
- [183] R. Clark, S. Wang, A. Markham, N. Trigoni, and H. Wen, "Vidloc: A deep spatio-temporal model for 6-dof video-clip relocalization," in *Proceedings of the IEEE Conference on Computer Vision and Pattern Recognition*, 2017, pp. 6856–6864.